Fig. 1

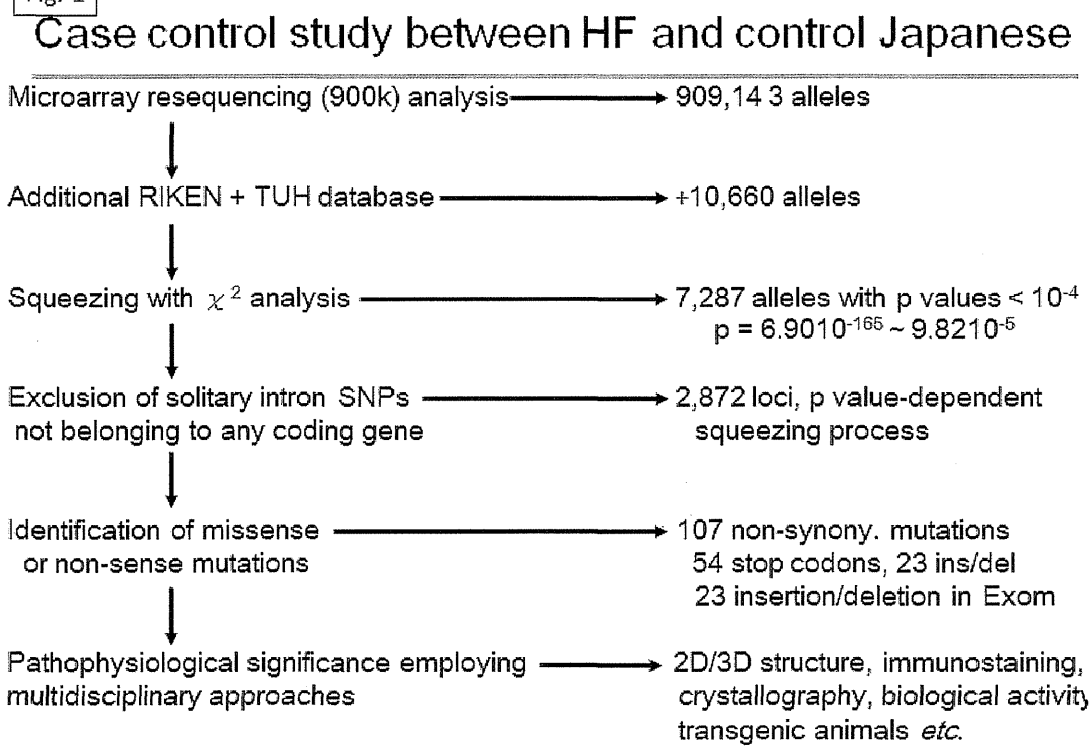
Case control study between HF and control Japanese
Microarray resequencing (900k) analysis
909,14 3 alleles
Additional RIKEN + TUH database
+10,660 alleles
Squeezing with χ^2 analysis
7,287 alleles with p values < 10^{-4}
p = 6.9010^{-165} ~ 9.8210^{-5}
Exclusion of solitary intron SNPs not belonging to any coding gene
2,872 loci, p value-dependent squeezing process
Identification of missense or non-sense mutations
107 non-synony. mutations
54 stop codons, 23 ins/del
23 insertion/deletion in Exom
Pathophysiological significance employing multidisciplinary approaches
2D/3D structure, immunostaining, crystallography, biological activity transgenic animals *etc.*

Fig. 2

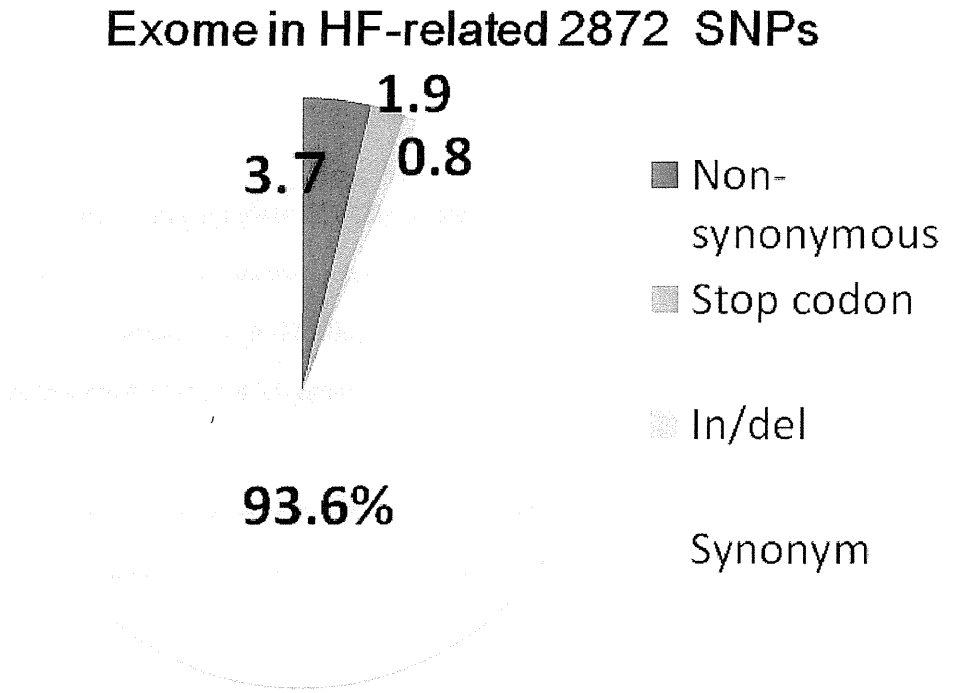
Exome in HF-related 2872 SNPs
1.9
3.7
0.8
93.6%
Non-synonymous
Stop codon
In/del
Synonym

Fig. 3

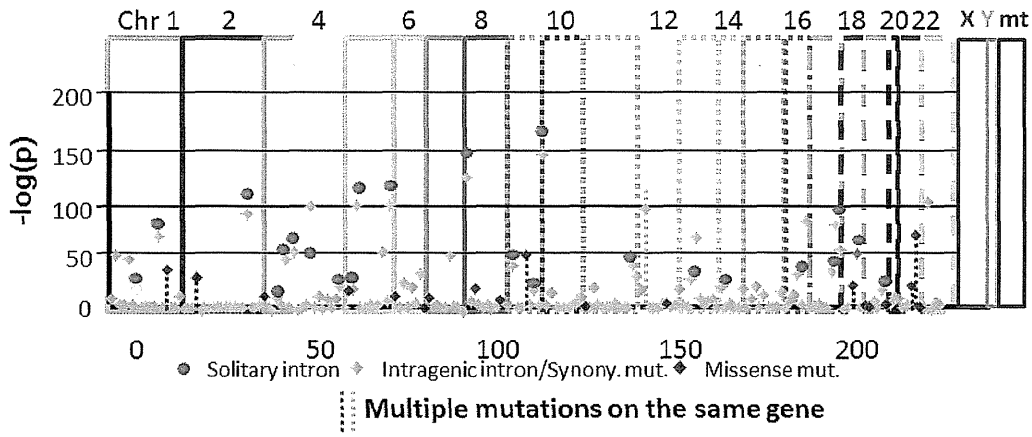
Chr 1 2 4 6 8 10 12 14 16 18 2022 X Y mt
-log(p)
200
150
100
50
0
0 50 100 150 200
Solitary intron
Intragenic intron/Synony. mut.
Missense mut.
Multiple mutations on the same gene

Fig. 4

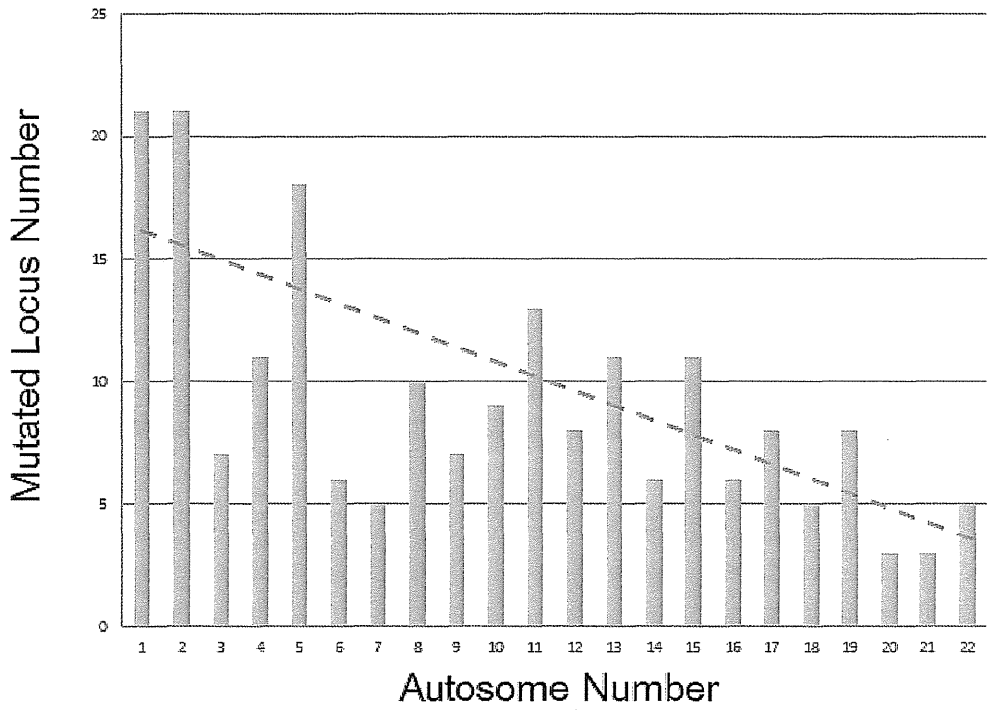
Mutated Locus Number
25
20
15
10
5
0
1 2 3 4 5 6 7 8 9 10 11 12 13 14 15 16 17 18 19 20 21 22
Autosome Number

Addendum

This monograph was planned to be published within 2012, but was delayed to Sep. 2013. During the interval, both case number and gene analyses proceeded and the authors add recent up-to-date SNP in March 2014 and displayed below. HF-related GWAS was reported in European American and African American (Smith *et al., Circulation, cardiovascular genet.,*3: 256-66, 2010) and some SNPs were coincided with our results in part (* ref. column in the table). Also, note that recent paper whole-exome sequencing (Yang *et al., N Engl J Med,* 369:1502-11; 2013) indicated 25% confirmation with in consecutive families with neurological diseases mainly.

E-mail address to TT was changed to toyo3terry@gmail.com.

Heart failure (HF)-related nuclear and mitochonsrial genome-wide association study (GWAS) in each chromosome and mitochondrion

chr. Number	gene number	approx. length (Mbp)	sequenced length	HF-realted allele #	HF/length (Mbp)	missense aa	nonsyn/ ORF	in/del, stop or ncRNA	total iSNP	total syn.	total CNV	ref.
1	>3000	240	~90%	45865	191	458	15.3%	228	39084	483	18213	*
2	>2500	240	~95%	56452	232	218	8.7%	175	40375	372	15969	*
3	1900	200	~95%	12579	64	30	1.6%	66	16773	59	3209	*
4	1600	190	~95%	26712	141	75	4.7%	49	11364	119	14375	
5	1700	180	> 95%	56291	313	193	11.4%	151	36541	304	4013	
6	1900	170	> 95%	48149	198	203	10.7%	218	13493	326	18213	
7	1800	150	> 95%	20389	136	97	5.4%	89	8989	181	11673	*
8	1400	140	> 95%	48527	347	28	2.0%	197	19211	0	13431	*
9	>1400	130	> 85%	41451	319	94	6.7%	148	3983	208	10653	*
10	>1400	130	> 95%	25083	193	70	5.0%	122	9960	65	6899	*
11	2000	130	> 95%	1480	11.0	12	0.6%	7	1141	20	379	*
12	1600	130	> 95%	42750	329	206	12.9%	159	17312	415	10170	*
13	800	110	> 80%	34063	310	76	9.5%	112	18242	138	9042	
14	1200	100	> 80%	27849	278	127	10.6%	116	14150	206	8341	
15	1200	100	> 80%	26121	261	122	10.2%	155	21526	261	6396	*
16	1300	90	> 85%	23237	258	46	3.5%	119	21166	251	7259	
17	1600	80	> 95%	9513	119	146	9.1%	105	8611	174	2295	
18	600	70	> 95%	11191	160	65	10.8%	31	6473	67	2636	
19	>1700	60	> 85%	7624	127	195	11.5%	106	5565	227	3391	*
20	900	60	> 90%	22807	360	179	19.9%	118	17587	217	6041	
21	400	40	> 70%	12537	313	57	14.3%	91	12340	88	3277	
22	800	40	~70%	11411	285	142	17.8%	121	10903	161	2925	
X	>1400	150	~95%	42323	282	220	15.7%	110	31142	313	9301	
Y	>366	50	~50%	366	7	0	0.0%	1	81	1	?	
mt	37	0.016569	complete	119	150602	25	150602.0%	2	0	63	5	
Umbiguous	116											
No assembly	44											
Sum	**~35000**	**2.93 Bbp**	**50~100%**	**~663800**		**3084**		**>2796**	**>385931**	**>4718**	**>188106**	

Cardiovascular Research (2013) 99, 461–470
doi:10.1093/cvr/cvt122

Deficiency of senescence marker protein 30 exacerbates angiotensin II-induced cardiac remodelling

Tomofumi Misaka[1], Satoshi Suzuki[1], Makiko Miyata[1], Atsushi Kobayashi[1], Tetsuro Shishido[2], Akihito Ishigami[3], Shu-ichi Saitoh[1], Masamichi Hirose[4], Isao Kubota[2], and Yasuchika Takeishi[1]*

[1]Department of Cardiology and Hematology, Fukushima Medical University, 1 Hikarigaoka, Fukushima 960-1295, Japan; [2]First Department of Internal Medicine, Yamagata University School of Medicine, Yamagata, Japan; [3]Molecular Regulation of Aging, Tokyo Metropolitan Institute of Gerontology, Tokyo, Japan; and [4]Department of Molecular and Cellular Pharmacology, Iwate Medical University School of Pharmaceutical Science, Iwate, Japan

Received 17 December 2012; revised 11 May 2013; accepted 15 May 2013; online publish-ahead-of-print 30 May 2013

Time for primary review: 37 days

Aims Ageing is an important risk factor of cardiovascular diseases including heart failure. Senescence marker protein 30 (SMP30), which was originally identified as an important ageing marker protein, is assumed to act as a novel anti-ageing factor in various organs. However, the role of SMP30 in the heart has not been previously explored. In this study, our aim was to elucidate the functional role of SMP30 on cardiac remodelling.

Methods and results SMP30 knockout (KO) mice and wild-type (WT) mice were subjected to continuous angiotensin II (Ang II) infusion. After 14 days, the extent of cardiac hypertrophy and myocardial fibrosis was significantly higher in SMP30-KO mice than in WT mice. Echocardiography revealed that SMP30-KO mice had more severely depressed systolic and diastolic function with left ventricular dilatation compared with WT mice. Generation of reactive oxygen species related with activation of nicotinamide adenine dinucleotide phosphate-oxidase was greater in SMP30-KO mice than in WT mice. The number of deoxynucleotidyl transferase-mediated dUTP nick end-labelling positive nuclei was markedly increased in SMP30-KO mice with activation of caspase-3, increases in the Bax to Bcl-2 ratio and phosphorylation of c-Jun N-terminal kinase compared with WT mice. Furthermore, the number of senescence-associated β-galactosidase-positive cells was significantly increased via up-regulation of p21 gene expression in SMP30-KO mice compared with WT mice.

Conclusion This study demonstrated the first evidence that deficiency of SMP30 exacerbates Ang II-induced cardiac hypertrophy, dysfunction, and remodelling, suggesting that SMP30 has a cardio-protective role in cardiac remodelling with anti-oxidative and anti-apoptotic effects in response to Ang II.

Keywords Senescence marker protein 30 (SMP30) • Ageing • Remodelling • Oxidative stress • Apoptosis

1. Introduction

The prevalence and mortality rate of heart failure dramatically increase in older people, and ageing is one of the risk factors for cardiovascular events.[1] With ageing, the heart shows changes in cardiac structure and function. Age-associated cardiac remodelling includes an enlargement of cardiomyocyte size, loss of myocytes due to apoptosis or necrosis, and increase of matrix connective tissue. These age-associated cardiac changes seem to be relevant to the steep increases in left ventricular hypertrophy, diastolic dysfunction, and subsequent heart failure.[2]

Oxidative stress is considered to be an important factor in controlling heart ageing.[3] It is well known that the renin–angiotensin system (RAS) is a central component of the physiological and pathological responses of the cardiovascular system. Activation of RAS is a significant driver of oxidative stress and is involved in age-related cardiac remodelling. Angiotensin II (Ang II), the primary effector molecule of RAS, contributes not only to vasoconstriction and hypertension, but also to cardiac hypertrophy, remodelling, and heart failure. Therefore, Ang II signalling appears to play a critical role in heart ageing.

* Corresponding author. Tel: +81 245471190; fax: +81 245481821. Email: takeishi@fmu.ac.jp

Published on behalf of the European Society of Cardiology. All rights reserved. © The Author 2013. For permissions please email: journals.permissions@oup.com.

Senescence marker protein 30 (SMP30), a 34-kDa protein, was originally identified as a novel ageing marker protein in rat liver, whose expression decreases androgen-independently with age.[4] SMP30 transcripts are detected in almost all organs, and the SMP30 gene is highly conserved among numerous animal species including humans.[5] Intracellular localization of SMP30 is in the cytoplasm and perinuclear regions, and SMP30 exists in multiple forms under physiological conditions.[6] It has been demonstrated that SMP30 plays multifunctional roles as Ca^{2+} regulator (named as regucalcin),[7] anti-oxidant,[8] and enzymatic ability to hydrolyze di-isopropyl phosphorofluoridate.[9] Recently, SMP30 has been determined as gluconolactonase, which is involved in ascorbic acid (vitamin C) biosynthesis in mammals, whereas human beings are unable to synthesize vitamin C *in vivo* because of mutations in L-gulonolactone oxidase.[10]

SMP30-knockout (KO) mice have been generated[11] and showed a shorter life span than that of the wild-type (WT) mice on a vitamin C-deficient diet.[12] Using SMP30-KO mice, recent reports have demonstrated that SMP30 functions to protect cells from apoptosis in the liver[11] and that SMP30 has protective effects against age-associated oxidative stress in the brain[13] and lungs.[14] Furthermore, SMP30-KO mice have shown accelerated senescence in the kidney[15] and the worsening of glucose tolerance.[16] Taken together, SMP30 is assumed to behave as an anti-ageing factor. However, the role of SMP30 in the heart has not been previously explored.

We hypothesized that SMP30 has cardio-protective functions from harmful stimuli with anti-oxidative and anti-apoptotic effects. To test the hypothesis, we used SMP30-KO mice to examine the effects of SMP30 on Ang II-induced cardiac hypertrophy and remodelling *in vivo*.

2. Methods

For additional detailed methods, please see Supplementary material online..

2.1 Animal protocol

SMP30-KO (C57BL/6 background) mice were established as previously reported.[11] Drinking water containing vitamin C (1.5 g/L) was provided for the SMP30-KO mice to avoid vitamin C deficiency due to their inability to synthesize vitamin C *in vivo*.[10] After anaesthetizing the mice by i.p. injection of pentobarbital (50 mg/kg body weight), an osmotic minipump (ALZET micro-osmotic pump MODEL 1002, DURECT Co., Cupertino, CA, USA) was subcutaneously implanted, and Ang II (800 ng/kg/min) was continuously infused for 14 days.[17,18] Controls were administered saline. The investigations conformed to the *Guide for the Care and Use of Laboratory Animals* published by the US National Institutes of Health (NIH publication, 8th Edition, 2011). Our research protocol was approved by the institutional review board, and all animal experiments were conducted in accordance with the guidelines of Fukushima Medical University Animal Research Committee.

2.2 Measurement of vitamin C

Total vitamin C levels in the heart were measured by the dinitrophenylhydrazine method according to the manufacturer's protocol (SHIMA Laboratories Co. Ltd., Tokyo, Japan).[19]

2.3 Measurements of blood pressure and heart rate

Mice were implanted with a radiotelemetry probe (TA11PA-C22, Data Sciences International, St Paul, MN, USA) under i.p. anaesthesia by pentobarbital (50 mg/kg body weight) as described previously.[20] After a recovery phase of 10 days, basal arterial pressure and heart rate (HR) were started to recorded. After the measurement of control, Ang II was subcutaneously infused via an osmotic minipump, and the data were recorded.

2.4 Echocardiography

Transthoracic echocardiography was performed using Vevo 2100 High-Resolution *In Vivo* Imaging System (Visual Sonics, Inc., Toronto, Canada) with a high-resolution 40-MHz imaging transducer as previous reports described.[21,22] Mice were lightly anaesthetized by titrating isoflurane (0.5–1.5%) to achieve an HR of ~400 b.p.m., and all the measurements were obtained from three cardiac cycles.

2.5 Cardiac catheterization

The cardiac catheterization was performed as described previously.[23] Briefly, mice were anaesthetized by i.p. injection of 2,2,2-tribromo-ethanol (250 mg/kg body weight), the right carotid artery was cannulated with the micropressure transducer (samba preclin 420 LP, Samba Sensors AB, Gothenburg, Sweden) into the left ventricle. Adequacy of anaesthesia was monitored by HR, aortic blood pressure, and respiratory rate as well as the absence of reactions of painful stimuli. The data were measured using the Labscribe 2 software (iWorx Systems, Inc., Dover, NH, USA).

2.6 Histopathological analysis

After continuous infusion of Ang II or saline for 14 days, mice were sacrificed by cervical dislocation and hearts were rapidly excised. The paraffin-embedded heart sections were stained with haematoxylin and eosin or Elastica-Masson. The cross-sectional area of cardiomyocyte and fibrosis fraction was measured using the NIH ImageJ software (National Institutes of Health, Bethesda, MD, USA) and Adobe Photoshop CS2 (Adobe, San Jose, CA, USA).[24]

In immunohistochemical analysis, the paraffin-embedded sections were incubated with anti-SMP30 antibody (SHIMA Laboratories Co. Ltd., Tokyo, Japan) with a dilution of 1:200 or negative control (normal serum). The sections were stained with horseradish peroxidase-conjugated secondary antibody (Histofine Simple Stain Mouse MAX PO (R), Nichirei Biosciences, Inc., Tokyo, Japan) and diaminobenzidine etrahydrochloride, and counterstained with haematoxylin.

2.7 Assessment of reactive oxygen species generation

The fresh-frozen heart sections were incubated with 10 μmol/L dihydroethidium (DHE, Sigma-Aldrich Co., St Louis, MO, USA).[25,26] The fluorescent images were acquired using fluorescence microscope (Olympus IX71, OLYMPUS Optical Co., Tokyo, Japan) and the mean DHE fluorescence intensity of cardiomyocytes was quantitated with the NIH imageJ software.[26] In addition, 10 mmol/L apocynin, a nicotinamide adenine dinucleotide phosphate (NADPH) oxidase inhibitor, was provided in drinking water with Ang II continuous infusion, and reactive oxygen species (ROS) generation was evaluated by DHE staining.[27]

2.8 Western blotting

Total protein was extracted from the snap-frozen left ventricle using Cell Lysis Buffer (Cell Signaling Technology, Inc., Beverly, MA, USA) with Protease Inhibitor Cocktail (BD Biosciences, San Jose, CA, USA) as previous reports described.[24] The primary antibodies were as follows: anti-SMP30, anti-67^{phox}, anti-Bax, anti-Bcl-2, anti-phospho-stress-activated protein kinase/c-Jun N-terminal kinase (SAPK/JNK, Thr183/Tyr185), anti-SAPK/JNK (Cell Signaling Technology, Inc.), anti-activated-caspase-3 (Bioworld Technology, Inc., Minneapolis, MN, USA), and mouse anti-β-actin (Santa Cruz Biotechnology, Inc.). The signals from immunoreactive bands were visualized by an Amersham ECL system (Amersham Pharmacia Biotech UK Ltd., Buckinghamshire, UK) and quantified using densitometric analysis.

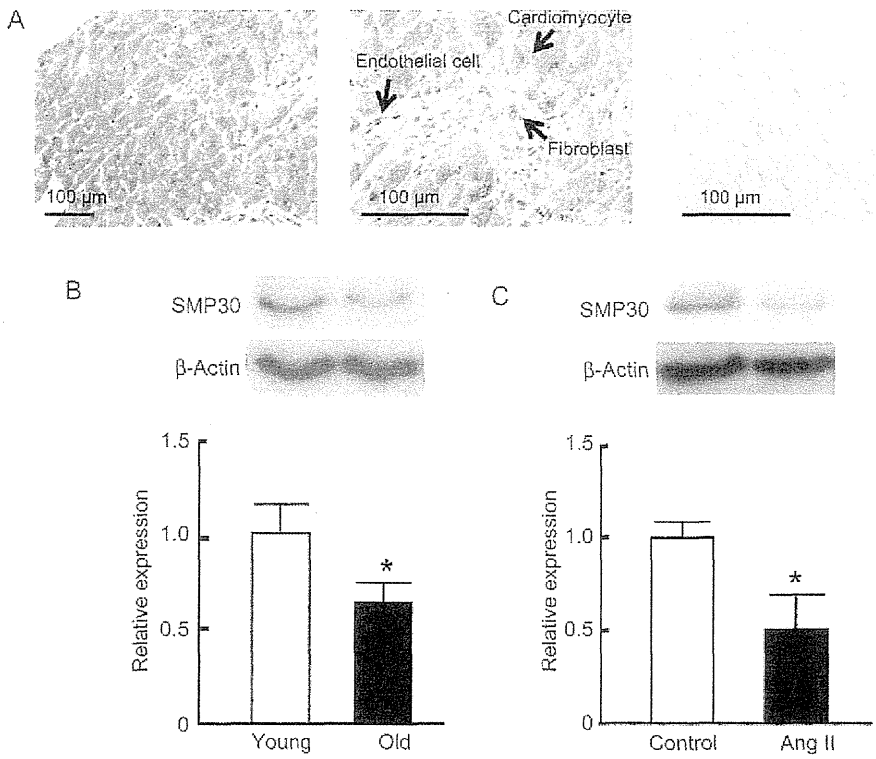

Figure 1 SMP30 expression in heart tissue. (*A*) SMP30 is expressed in cardiomyocytes, fibroblasts, and vascular endothelial cells (left, magnification ×200; middle, ×400). Right panel indicates negative control (×400). (*B*) Cardiac SMP30 expression was significantly decreased by 40% at 12-month-old WT mice (old) compared with 3-month-old WT mice (young). (*C*) Cardiac SMP30 expression was significantly decreased by 50% after Ang II infusion for 14 days in WT mice. Results are mean ± SD from 3 mice in each group. $^*P < 0.05$ vs. young mice or control.

2.9 *In vivo* terminal deoxynucleotidyl transferase-mediated dUTP nick end- labellingassay

Apoptosis was detected by the terminal deoxynucleotidyl transferase-mediated dUTP nick end-labelling (TUNEL) method (CardioTACS *In Situ* Apoptosis Detection Kit, Trevigen, Inc., Gaithersburg, MD, USA) according to the manufacturer's instructions. TUNEL-positive nuclei were counted, and then expressed as a per cent of the total nuclei.[28]

2.10 Senescence-associated β-galactosidase activity

Senescence-associated β-galactosidase (SA-β-gal) staining was performed according to the manufacturer's protocol (BioVision, Inc., Mountain View, CA, USA).[29] SA-β-gal-positive cardiomyocytes were visualized as blue colour under light microscopy, and positive cells for SA-β-gal activity were counted.

2.11 Reverse transcription polymerase chain reaction

Total RNA was extracted from the snap-frozen left ventricle using TRIzol reagent (Invitrogen, Carlsbad, CA, USA).[28] Reverse transcription polymerase chain reaction (RT–PCR) was performed using the PrimeScript RT–PCR Kit (Takara Bio, Inc., Otsu, Japan) according to the manufacturer's instructions. Primers were designed on the basis of GenBank sequences (p21, NM_001111099 and β-actin, NM_007393). The optical density of the bands was quantified using the NIH image] software.

2.12 Statistical analysis

All data were expressed as mean ± SD. Comparisons of vitamin C levels at basal conditions between WT mice and SMP30-KO mice were performed by an unpaired *t*-test. All other parameters were evaluated by two-way analysis of variance followed by multiple comparisons with the Bonferroni test using SPSS Statistics 17.0 (SPSS Japan, Inc., Tokyo, Japan). A probability value < 0.05 was considered statistically significant.

3. Results

3.1 Vitamin C levels of the heart tissue in WT mice and SMP30-KO mice

First, we measured vitamin C levels of the heart tissue in basal conditions. To avoid vitamin C deficiency, drinking water containing sufficient vitamin C was supplied for SMP30-KO mice because SMP30-KO mice were unable to synthesize vitamin C due to the lack of gluconolactonase.[10] The tissue concentrations of the vitamin C level were not significantly different between WT mice and SMP30-KO mice (45.7 ± 7.0 vs. 44.5 ± 10.2 μg/g tissue).

3.2 SMP30 expression in the heart tissue

Immunostaining revealed that SMP30 was expressed in cardiomyocytes, fibroblasts, and vascular endothelial cells in WT mice on the basis of cellular morphological characteristics (*Figure 1A*).[30] We confirmed the decrease in SMP30 expression with ageing in the WT mouse heart as

Table 1 Gravimetric and hemodynamic data of WT and SMP30-KO mice

	Control		Ang II	
	WT	SMP30-KO	WT	SMP30-KO
Gravimetric data				
BW, g	26.7 ± 1.1	27.8 ± 1.6	25.6 ± 1.5	27.2 ± 2.2
HW/TL, mg/mm	6.1 ± 0.6	6.5 ± 0.5	7.5 ± 0.6**	8.4 ± 1.0**†
LVW/TL, mg/mm	4.2 ± 0.5	4.6 ± 0.3	5.7 ± 0.5**	6.7 ± 0.9**††
Telemetry blood pressure				
HR, b.p.m.	612 ± 48	627 ± 50	593 ± 24	607 ± 65
SBP, mmHg	115.5 ± 12.4	114.8 ± 10.8	140.8 ± 8.6**	144.1 ± 13.7**
DBP, mmHg	85.1 ± 9.4	89.9 ± 9.6	129.4 ± 7.0**	128.6 ± 10.6**
MAP, mmHg	97.8 ± 11.6	99.9 ± 10.4	119.0 ± 6.2**	115.2 ± 9.7**
Echocardiography				
LVEDD, mm	3.77 ± 0.37	3.77 ± 0.38	3.68 ± 0.31	4.26 ± 0.21**††
LVESD, mm	2.52 ± 0.32	2.42 ± 0.42	2.52 ± 0.35	3.12 ± 0.33**††
FS, %	33.2 ± 4.4	33.7 ± 4.1	31.8 ± 4.7	25.9 ± 5.2**††
Catheterization				
LVEDP, mmHg	5.2 ± 1.6	6.0 ± 1.7	9.8 ± 1.0*	11.7 + 3.0**
max d*P*/d*t*, mmHg/s	11 556 ± 850	10 977 ± 940	11 675 ± 999	7303 ± 1107**††
min d*P*/d*t*, mmHg/s	8140 ± 668	8247 ± 384	7582 ± 1408	4804 ± 1897*†
Tau, ms	4.8 ± 2.0	4.3 ± 0.3	6.3 ± 1.9**	8.3 ± 1.9**

Data are presented as mean ± SD from 10 to 15 mice in each group.
BW, body weight; HW, heart weight; LVW, left ventricular weight; TL, tibial length; HR, heart rate; SBP, systolic blood pressure; DBP, diastolic blood pressure; MAP, mean arterial pressure; LVEDD, left ventricular end-diastolic dimension; LVESD, left ventricular end-systolic dimension; FS, fractional shortening; LVEDP, left ventricular end-diastolic pressure; max and min d*P*/d*t*, maximal and minimal rates of left ventricular pressure development, respectively; Tau, time constant of left ventricular isovolumic relaxation.
*$P < 0.05$ and **$P < 0.01$ vs. control in the same strain mice; †$P < 0.05$ and ††$P < 0.01$ vs. Ang II-infused WT mice.

described previously in other organs.[4] Cardiac SMP30 was significantly decreased by 40% at 12-month-old WT mice compared with 3-month-old WT mice ($P < 0.05$, *Figure 1B*). Additionally, cardiac expression of SMP30 was significantly decreased by 50% after Ang II infusion for 14 days in 3-month-old WT mice, suggesting that the expression of SMP30 may alter in cardiovascular diseases ($P < 0.05$, *Figure 1C*).

3.3 Effect of SMP30 deficiency on Ang II-induced cardiac hypertrophy and fibrosis

As shown in *Table 1*, heart weight (HW) and left ventricular weight (LVW) corrected by the tibial length (TL) were similar between control WT mice and SMP30-KO mice. After Ang II infusion, the ratios of HW to TL and LVW to TL were significantly higher in SMP30-KO mice than in WT mice ($P < 0.05$ and $P < 0.01$, respectively), although the blood pressure was similarly elevated in both Ang II-infused WT mice and SMP30-KO mice by telemetry blood pressure monitoring (*Table 1*).

Histological examination showed that Ang II-infused SMP30-KO mice had substantial left ventricular hypertrophy with left ventricular dilatation compared with Ang II-infused WT mice, which suggested eccentric hypertrophy in Ang II-infused SMP30-KO mice compared with concentric hypertrophy in Ang II-infused WT mice (*Figure 2A*, top). The cardiomyocyte cross-sectional area was significantly larger in Ang II-infused SMP30-KO mice than in Ang II-infused WT mice (399 ± 17 vs. 372 ± 11 μm^2, $P < 0.01$, *Figure 2A*, middle and *B*). Additionally, *ex vivo* analysis demonstrated that cell width, length, and surface area of isolated cardiomyocytes were significantly greater in SMP30-KO mice than in WT mice after Ang II stimulation (Supplementary material online, *Figure S1*). The degree of cardiac fibrosis was significantly higher in Ang II-infused SMP30-KO mice than in Ang II-infused WT mice (6.4 ± 0.8 vs. 7.5 ± 0.7%, $P < 0.01$, *Figure 2A*, bottom and *C*). These data revealed that the deficiency of SMP30 exacerbates Ang II-induced cardiac hypertrophy and fibrosis, independently of blood pressure.

3.4 Effect of SMP30 deficiency on Ang II-induced cardiac dysfunction

As shown in *Table 1*, there were no differences in cardiac function between WT mice and SMP30-KO mice under basal conditions. Echocardiography showed that left ventricular end-diastolic and end-systolic dimensions were enlarged and fractional shortening was reduced in SMP30-KO mice compared with WT mice at 14 days after Ang II infusion ($P < 0.01$, *Table 1* and Supplementary material online, *Table S1* and *Figure S2*, top). The left ventricular mass was greater in Ang II-infused SMP30-KO mice than in Ang II-infused WT mice, which was concordant with the histological findings ($P < 0.01$). Ang II-infused SMP30-KO mice had significantly higher peak E velocity, *E*/*A*, and *E*/*E'* compared with Ang II-infused WT mice (Supplementary material online, *Table S1* and *Figure S2*, middle and bottom). The mitral inflow showed the restrictive pattern in Ang II-infused SMP30-KO mice in contrast to the relaxation abnormality pattern or the pseudo-normalization pattern in Ang II-infused WT mice. These echocardiographic data revealed that left ventricular systolic and diastolic functions were remarkably depressed in SMP30-KO mice compared with WT mice after Ang II infusion.

Haemodynamic assessment by cardiac catheterization showed that max d*P*/d*t* and min d*P*/d*t* were significantly lower in SMP30-KO mice than in WT mice after Ang II infusion ($P < 0.01$ and $P < 0.05$,

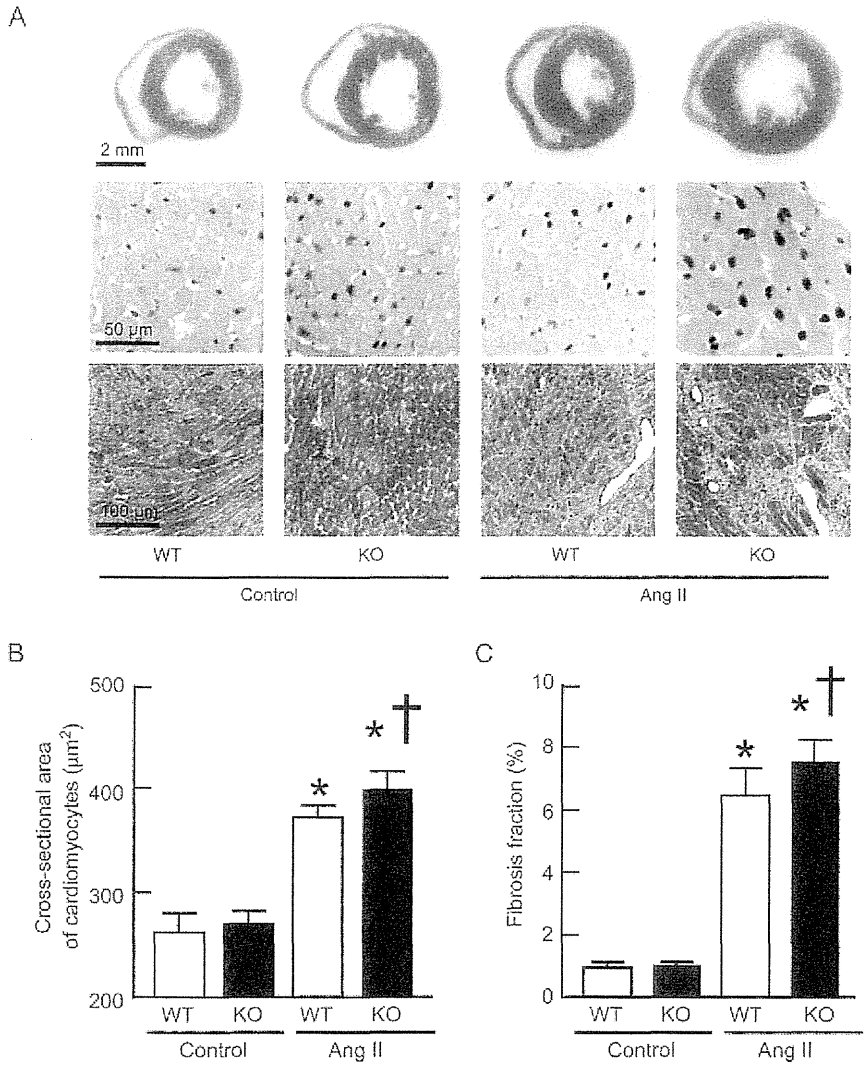

Figure 2 Cardiac hypertrophy and fibrosis in WT and SMP30-KO mice after Ang II infusion. (*A*) Representative images of light micrographs of hearts from WT and SMP30-KO mice with and without Ang II infusion (top). Haematoxylin and eosin staining of myocardial cross-sections (middle). Elastica-Masson staining of myocardial sections (bottom). (*B*) Quantitative analysis of the cross-sectional area of cardiomyocytes from the left ventricle. (*C*) The per cent area of myocardial interstitial fibrosis in the left ventricle. Data are presented as mean ± SD from 6 to 8 mice in each group. *$P < 0.01$ vs. control in the same strain mice; †$P < 0.01$ vs. Ang II-infused WT mice.

respectively), supporting that cardiac systolic and diastolic functions were more severely depressed in SMP30-KO mice (*Table 1*).

3.5 Effect of SMP30 deficiency on Ang II-induced myocardial oxidative stress

We examined myocardial oxidative stress by DHE staining which indicates the O_2levels of living cells because oxidative stress is considered to be one of the important mechanisms of heart failure and cardiac remodelling. Although Ang II infusion dramatically increased the ROS generation in both WT mice and SMP30-KO mice, the ROS generation in Ang II-infused SMP30-KO mice was significantly greater than in Ang II-infused WT mice ($P < 0.01$, *Figure 3A*). In addition, we found that the level of superoxide generation was significantly decreased in Ang II-infused WT mice with apocynin treatment, compared with that of Ang II-infused WT mice without apocynin treatment ($P < 0.01$, *Figure 3A*). As well as WT mice, SMP30-KO mice revealed that Ang II-induced superoxide generation was significantly down-regulated by apocynin treatment ($P < 0.01$, *Figure 3A*).

To investigate the involvement of NADPH oxidase in Ang II-induced ROS generation, we examined the expression of $p67^{phox}$ subunit of NADPH oxidase by western blotting. The expression levels of $p67^{phox}$ were significantly elevated in Ang II-infused SMP30-KO mice compared with Ang II-infused WT mice ($P < 0.01$, *Figure 3B*). These data suggested that the deficiency of SMP30 increased Ang II-induced myocardial oxidative stress via up-regulation of NADPH oxidase.

3.6 Effect of SMP30 deficiency on Ang II-induced apoptosis

As previously demonstrated, SMP30 has anti-apoptotic effects in other organs.[11] We, therefore, checked apoptosis using TUNEL staining

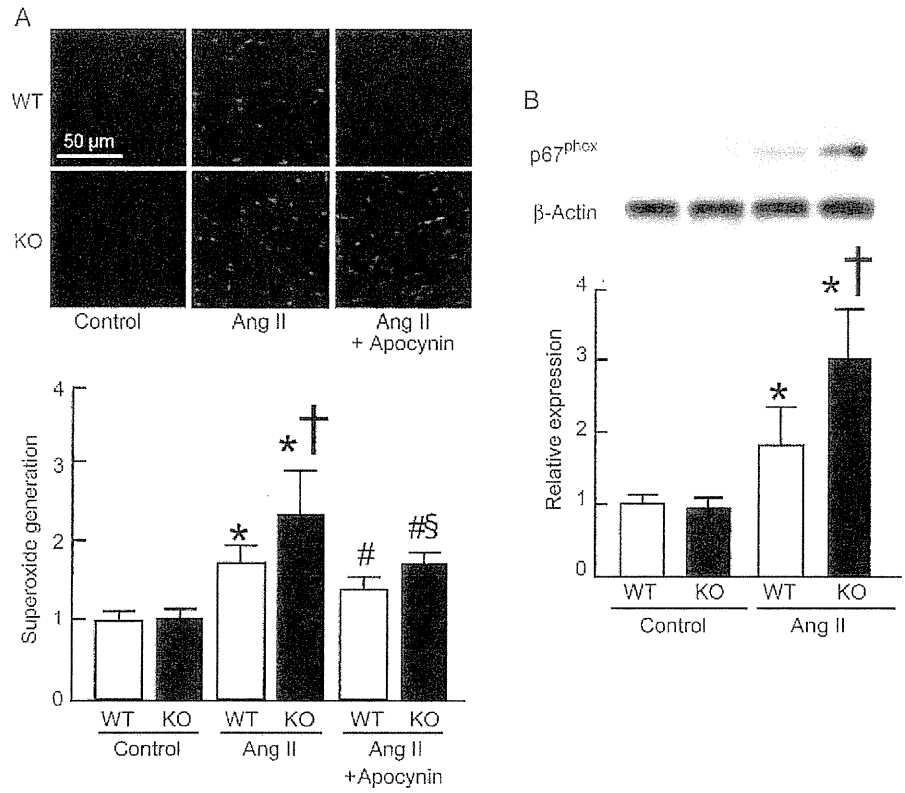

Figure 3 Myocardial oxidative stress in WT and SMP30-KO mice after Ang II infusion. (*A*) Upper panels show representative DHE staining of frozen left ventricular tissues. Lower bar graphs show quantification of superoxide generation. (*B*) Expression of $p67^{phox}$ of NADPH oxidase subunits was analysed by western blotting. Expression levels were expressed relative to those of β-actin. Results are mean ± SD from 6 to 10 mice in each group. $^{*}P < 0.01$ vs. control in the same strain mice; $^{\dagger}P < 0.01$ vs. Ang II-infused WT mice. $^{\#}P < 0.05$ vs. Ang II-infused mice in the same strain; $^{\S}P < 0.05$ vs. Ang II-infused WT mice with apocynin treatment.

(*Figure 4A*). After Ang II infusion, the numbers of TUNEL-positive nuclei including cardiomyocytes and non-cardyomyocytes were increased in both WT and SMP30-KO mice. The numbers of TUNEL-positive nuclei in Ang II-infused SMP30-KO mice were remarkably greater than in Ang II-infused WT mice, as shown in *Figure 4A* ($P < 0.01$).

Then, we examined signalling pathways of Ang II-induced apoptosis in the heart. Caspase-3 is a key mediator of apoptosis, and activation of caspase-3 leads to DNA injury and subsequently apoptotic cell death.[31] The activation of caspase-3 was induced by Ang II infusion in both WT and SMP30-KO mice, and the activation of caspase-3 in Ang II-infused SMP30-KO mice was significantly greater than in Ang II-infused WT mice ($P < 0.01$, *Figure 4B*). After Ang II infusion, Bax expression which functions as pro-apoptotic protein was increased, whereas the expression of anti-apoptotic protein Bcl-2 was decreased in both genotypes of mice. The ratio of Bax to Bcl-2 was significantly higher in Ang II-infused SMP30-KO mice than in Ang II-infused WT mice ($P < 0.01$, *Figure 4C*). Furthermore, we examined the involvement of SAPK/JNK which has a crucial role in cell apoptosis as one main subgroup of the mitogen-activated protein kinase family.[32] Phosphorylation activity of SAPK/JNK in Ang II-infused SMP30-KO mice was significantly increased compared with Ang II-infused WT mice ($P < 0.01$, *Figure 4D*). These findings demonstrated that SMP30 deficiency exacerbates Ang II-induced apoptosis through these signalling pathways.

3.7 Expression of senescence markers in SMP30-KO mice after Ang II infusion

Senescent cells can be identified by the expression of enzymatic SA-β-gal activity in left ventricular tissues (*Figure 5A*). SA β-gal activity was induced by Ang II stimulation. The numbers of SA β-gal-positive cells were significantly greater in Ang II-infused SMP30-KO mice than in Ang II-infused WT mice (1.7 ± 0.8 vs. $0.6 \pm 0.5/mm^3$, $P < 0.01$) as demonstrated in *Figure 5A*.

To evaluate the gene expression of cell cycle inhibitor to confirm senescence of cardiomyocytes, we analysed mRNA expression of p21 gene by RT–PCR (*Figure 5B*). Following Ang II infusion, the expression levels of p21 mRNA were increased in both WT mice and SMP30-KO mice. Compared with Ang II-infused WT mice, Ang II-infused SMP30-KO mice showed a significant increase in p21 expression ($P < 0.01$). These results indicate that deficiency of SMP30 induced cellular senescence after Ang II infusion by the p21-dependent pathway.

4. Discussion

Previous studies have shown that SMP30 acts as an anti-ageing factor, and SMP30 prevents oxidative stress and apoptosis in the liver, lungs, and brain.[11,13,14] However, the role of SMP30 in the heart has not

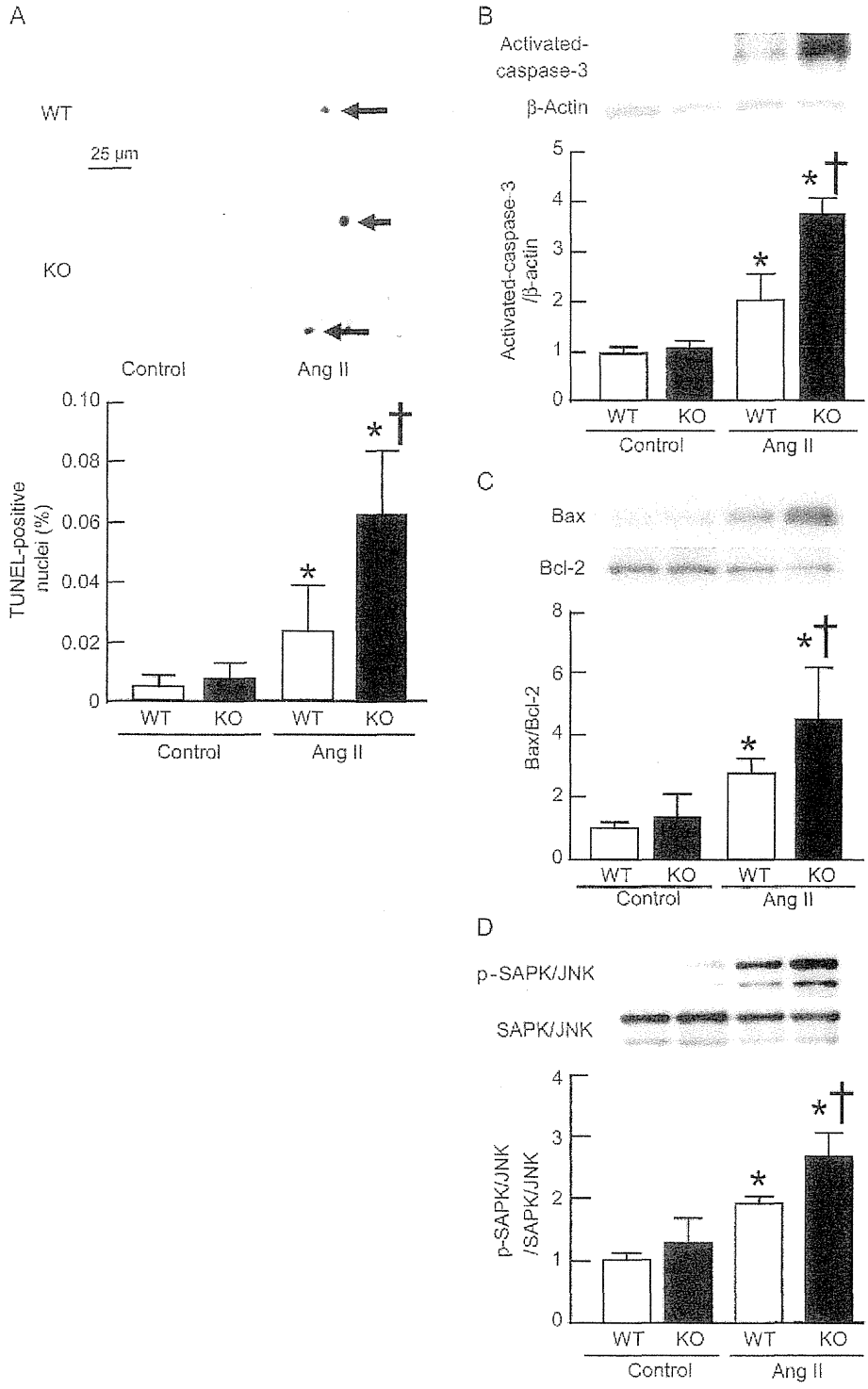

Figure 4 Apoptosis and apoptotic signalling pathways in WT and SMP30-KO mice after Ang II infusion. (*A*) Upper panels show representative images of TUNEL staining of left ventricular tissue sections. Lower bar graph shows the per cent of TUNEL-positive nuclei. (*B*) Activation of caspase-3 was examined by western blotting with anti-activated-caspase-3 antibody using myocardial samples. Expression levels of activated-caspase-3 were normalized by β-actin. (*C*) Expressions of Bax and Bcl-2 were analysed by western blotting. The Bax to Bcl-2 ratio was calculated and presented in the bar graph. (*D*) Phosphorylation activity of SAPK/JNK. Expressions of phosphorylated and total SAPK/JNK were analysed by western blotting. Relative expression levels of phosphorylated SAPK/JNK (P-SAPK/JNK) were expressed in relation to those of SAPK/JNK. Results are mean ± SD from 6 to 10 mice in each group. *$P < 0.01$ vs. control in the same strain mice; †$P < 0.01$ vs. Ang II-infused WT mice.

been investigated. In this study, we demonstrated the first evidence that deficiency of SMP30 exacerbates Ang II-induced cardiac hypertrophy, dysfunction, and adverse remodelling. Our results revealed that SMP30 has a cardio-protective role with anti-oxidative and anti-apoptotic effects in response to Ang II.

It has been well known that Ang II plays an important role in the development of pathological cardiac hypertrophy, remodelling, and subsequent heart failure.[33] Subcutaneous chronic infusion of Ang II induces cardiac hypertrophy and fibrosis with hypertension.[18,34] Ang II also stimulates NADPH oxidase to produce ROS,[35] and consequent myocardial oxidative stress is associated with the development of left ventricular remodelling and heart failure.[36] Furthermore, it has been considered that apoptosis plays an adverse role in cardiac remodelling and contributes to progressive myocardial dysfunction[37] and that Ang II exaggerates apoptotic responses in cardiomyocytes.[38] Interestingly, we observed that deficiency of SMP30 exacerbates Ang II-induced cardiac hypertrophy and fibrosis in SMP30-KO mice (*Table 1*, *Figure 2*, and Supplementary material online, *Figure S1*). Moreover, we found that Ang II-infused SMP30-KO mice showed left ventricular dilatation and depressed systolic function in addition to more severely impaired diastolic function compared with Ang II-infused WT mice, suggesting that the absence of SMP30 caused more progressive cardiac dysfunction and remodelling (*Table 1* and Supplementary material online, *Table S1* and *Figure S2*). These remarkable changes were independent of Ang II-induced hypertension because increased systemic blood pressure of SMP30-KO mice was similar to that of WT mice (*Table 1*). SMP30-KO mice had much more elevated NADPH oxidase-generated ROS by Ang II stimulation (*Figure 3*). In addition, SMP30-KO mice were more susceptible to Ang II-induced apoptosis associated with activation of caspase-3, increase in Bax, decrease in Bcl-2, and phosphorylation of SAPK/JNK (*Figure 4*). Although we were unable to show the direct observation of TUNEL-positive cardiomyocyte nuclei, apoptosis of non-cardiomyocytes plays an important role in Ang II-induced cardiac remodelling and dysfunction as previously reported.[39] These data indicate that SMP30 has a protective role against Ang II-associated cardiac hypertrophy, dysfunction, and remodelling by inhibiting oxidative stress and apoptosis.

SMP30 has been proposed as an important ageing marker, and the lack of SMP30 causes various dysfunctions of organs during ageing process.[11,13–15] Concerning the vitamin C biosynthesis pathway, similar to humans, SMP30-KO mice cannot synthesize vitamin C and SMP30-KO mice may mimic the human physiology closer than other rodents.[40] The potent anti-ageing and anti-oxidative actions of a low-calorie diet effectively suppressed the age-related down-regulation of SMP30, indicating that SMP30 expression was influenced by oxidative stress.[41] These previous reports suggest that SMP30 expression accounts for the age-associated deterioration of cellular function and the enhanced susceptibility to harmful stimuli in aged tissues. On the other hand, very few reports demonstrated cellular senescence of cardiomyocytes *in vivo*.[42,43] We demonstrated that Ang II could increase senescent cells detected by SA β-gal activity *in vivo*. Importantly, Ang II-induced cellular senescence was accompanied with markedly elevated p21 gene expression. SMP30-KO mice showed significantly increased SA β-gal-positive cells with elevated expression of p21 gene by Ang II stimulation, indicating that SMP30 inhibits premature cellular senescence through the signalling pathway of p21 in response to Ang II (*Figure 5*).

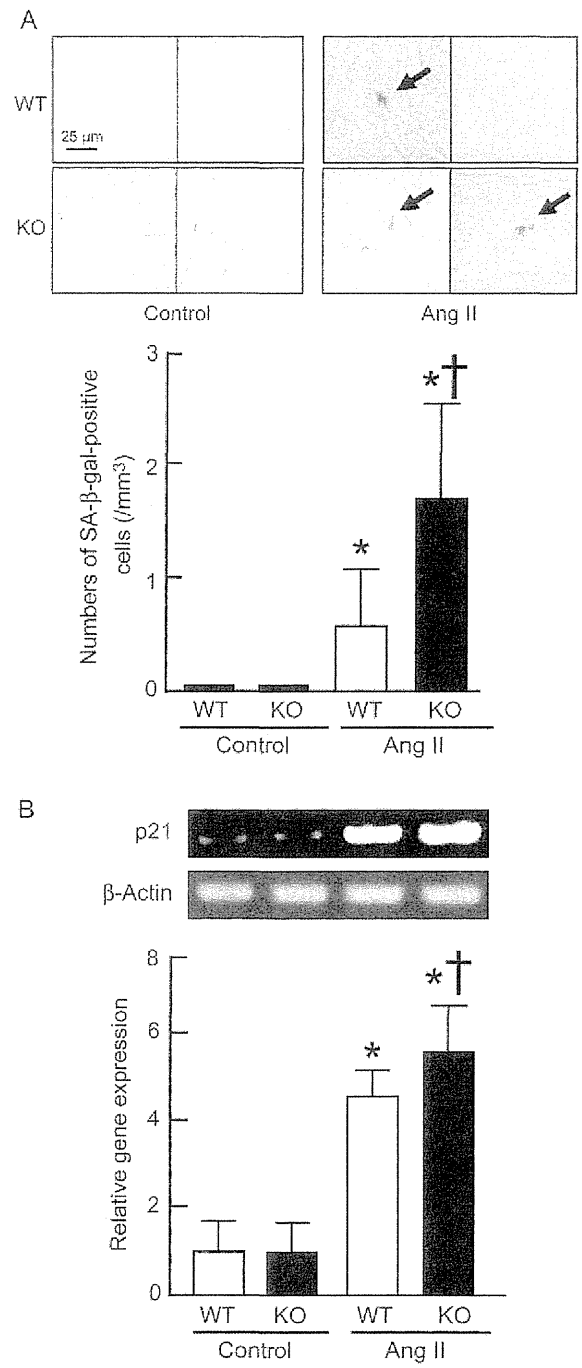

Figure 5 Senescence markers in hearts of WT and SMP30-KO mice after Ang II infusion. (*A*) Senescent cells were detected by SA β-gal staining of left ventricular tissue sections, and the numbers of SA β-gal-positive cells were counted. (*B*) The mRNA expression levels of p21 gene were analysed by RT–PCR. Expression levels of p21 gene were normalized by β-actin. Results are mean ± SD from 6 to 8 mice in each group. $^{*}P < 0.01$ vs. control in the same strain mice; $^{\dagger}P < 0.01$ vs. Ang II-infused WT mice.

There were no differences between WT mice and SMP30-KO mice under basal conditions at 12- to 16-week-old, but we observed that 12-month-old SMP30-KO mice showed exaggerated left ventricular hypertrophy, diastolic dysfunction, and myocardial fibrosis compared with 12-month-old WT mice (Supplementary material online, *Table S2*). One central role of SMP30 in the heart is considered to be the suppressive effect of ROS generation by inhibiting NADPH oxidase activation, as demonstrated in the present study (*Figure 3*). The suppressive role of SMP30 in oxidative stress contributes to the reduction of senescent marker expressions, suggesting that SMP30 prevents myocardial dysfunction from various stresses such as Ang II stimulation and ageing (Supplementary material online, *Figure S3*). Since detailed mechanisms have not been fully clarified, we should evaluate the cellular compartment specific effects of SMP30 in the future study.

5. Conclusions

In summary, deficiency of SMP30 adversely modifies Ang II-induced cardiac hypertrophy and remodelling through increase in oxidative stress and progression of apoptosis. These data provide that SMP30 has a protective role in cardiac remodelling and up-regulation of SMP30 could be a therapeutic target for treatment of heart failure.

Supplementary material

Supplementary material is available at *Cardiovascular Research* online.

Acknowledgements

We thank Ms. Emiko Kaneda for the excellent technical assistance.

Conflict of interest: none declared.

Funding

This study was supported in part by a grant-in-aid for Scientific Research (No. 24591100, Y.T.) from the Japan Society for the Promotion of Science.

References

1. Lakatta EG, Levy D. Arterial and cardiac aging: major shareholders in cardiovascular disease enterprises: part II: the aging heart in health: links to heart disease. *Circulation* 2003;**107**:346–354.
2. Lakatta EG. Arterial and cardiac aging: major shareholders in cardiovascular disease enterprises: part III: cellular and molecular clues to heart and arterial aging. *Circulation* 2003;**107**:490–497.
3. Wang M, Zhang J, Walker SJ, Dworakowski R, Lakatta EG, Shah AM. Involvement of NADPH oxidase in age-associated cardiac remodeling. *J Mol Cell Cardiol* 2010;**48**:765–772.
4. Fujita T, Uchida K, Maruyama N. Purification of senescence marker protein-30 (SMP30) and its androgen-independent decrease with age in the rat liver. *Biochim Biophys Acta* 1992;**1116**:122–128.
5. Fujita T, Mandel JL, Shirasawa T, Hino O, Shirai T, Maruyama N. Isolation of cDNA clone encoding human homologue of senescence marker protein-30 (SMP30) and its location on the X chromosome. *Biochim Biophys Acta* 1995;**1263**:249–252.
6. Arun P, Aleti V, Parikh K, Manne V, Chilukuri N. Senescence marker protein 30 (SMP30) expression in eukaryotic cells: existence of multiple species and membrane localization. *PLoS ONE* 2011;**6**:e16545.
7. Shimokawa N, Yamaguchi M. Molecular cloning and sequencing of the cDNA coding for a calcium-binding protein regucalcin from rat liver. *FEBS Lett* 1993;**327**:251–255.
8. Son TG, Kim SJ, Kim K, Kim MS, Chung HY, Lee J. Cytoprotective roles of senescence marker protein 30 against intracellular calcium elevation and oxidative stress. *Arch Pharm Res* 2008;**31**:872–877.
9. Little JS, Broomfield CA, Fox-Talbot MK, Boucher LJ, MacIver B, Lenz DE. Partial characterization of an enzyme that hydrolyzes sarin, soman, tabun, and diisopropyl phosphorofluoridate (DFP). *Biochem Pharmacol* 1989;**38**:23–29.
10. Kondo Y, Inai Y, Sato Y, Handa S, Kubo S, Shimokado K *et al.* Senescence marker protein 30 functions as gluconolactonase in L-ascorbic acid biosynthesis, and its knockout mice are prone to scurvy. *Proc Natl Acad Sci USA* 2006;**103**:5723–5728.
11. Ishigami A, Fujita T, Handa S, Shirasawa T, Koseki H, Kitamura T *et al.* Senescence marker protein-30 knockout mouse liver is highly susceptible to tumor necrosis factor-alpha- and Fas-mediated apoptosis. *Am J Pathol* 2002;**161**:1273–1281.
12. Ishigami A, Kondo Y, Nanba R, Onsawa T, Handa S, Kubo S *et al.* SMP30 deficiency in mice causes an accumulation of neutral lipids and phospholipids in the liver and shortens the life span. *Biochem Biophys Res Commun* 2004;**315**:575–580.
13. Son TG, Zou Y, Jung KJ, Yu BP, Ishigami A, Maruyama N *et al.* SMP30 deficiency causes increased oxidative stress in brain. *Mech Ageing Dev* 2006;**127**:451–457.
14. Sato T, Seyama K, Sato Y, Mori H, Souma S, Akiyoshi T *et al.* Senescence marker protein-30 protects mice lungs from oxidative stress, aging, and smoking. *Am J Respir Crit Care Med* 2006;**174**:530–537.
15. Yamura W, Imasawa T, Suganuma S, Ishigami A, Handa S, Kubo S *et al.* Accelerated tubular cell senescence in SMP30 knockout mice. *Histol Histopathol* 2006;**21**:1151–1156.
16. Hasegawa G, Yamasaki M, Kadono M, Tanaka M, Asano M, Senmaru T *et al.* Senescence marker protein-30/gluconolactonase deletion worsens glucose tolerance through impairment of acute insulin secretion. *Endocrinology* 2010;**151**:529–536.
17. Xue B, Pamidimukkala J, Lubahn DB, Hay M. Estrogen receptor-alpha mediates estrogen protection from angiotensin II-induced hypertension in conscious female mice. *Am J Physiol Heart Circ Physiol* 2007;**292**:H1770–H1776.
18. Kobayashi A, Ishikawa K, Matsumoto H, Kimura S, Kamiyama Y, Maruyama Y. Synergetic antioxidant and vasodilatory action of carbon monoxide in angiotensin II-induced cardiac hypertrophy. *Hypertension* 2007;**50**:1040–1048.
19. Tsao CS, Leung PY, Young M. Effect of dietary ascorbic acid intake on tissue vitamin C in mice. *J Nutr* 1987;**117**:291–297.
20. Carlson SH, Wyss JM. Long-term telemetric recording of arterial pressure and heart rate in mice fed basal and high NaCl diets. *Hypertension* 2000;**35**:E1–E5.
21. Du J, Liu J, Feng HZ, Hossain MM, Gobara N, Zhang C *et al.* Impaired relaxation is the main manifestation in transgenic mice expressing a restrictive cardiomyopathy mutation, R193H, in cardiac TnI. *Am J Physiol Heart Circ Physiol* 2008;**294**:H2604–H2613.
22. Wilson RM, De Silva DS, Sato K, Izumiya Y, Sam F. Effects of fixed-dose isosorbide dinitrate/hydralazine on diastolic function and exercise capacity in hypertension-induced diastolic heart failure. *Hypertension* 2009;**54**:583–590.
23. Kitahara T, Takeishi Y, Harada M, Niizeki T, Suzuki S, Sasaki T *et al.* High-mobility group box 1 restores cardiac function after myocardial infarction in transgenic mice. *Cardiovasc Res* 2008;**80**:40–46.
24. Arimoto T, Takeishi Y, Takahashi H, Shishido T, Niizeki T, Koyama Y *et al.* Cardiac-specific overexpression of diacylglycerol kinase zeta prevents Gq protein-coupled receptor agonist-induced cardiac hypertrophy in transgenic mice. *Circulation* 2006;**113**:60–66.
25. Takimoto E, Champion HC, Li M, Ren S, Rodriguez ER, Tavazzi B *et al.* Oxidant stress from nitric oxide synthase-3 uncoupling stimulates cardiac pathologic remodeling from chronic pressure load. *J Clin Invest* 2005;**115**:1221–1231.
26. Machii H, Saitoh S, Kaneshiro T, Takeishi Y. Aging impairs myocardium-induced dilation in coronary arterioles: role of hydrogen peroxide and angiotensin. *Mech Ageing Dev* 2010;**131**:710–717.
27. Matsushima S, Kinugawa S, Yokota T, Inoue N, Ohta Y, Hamaguchi S *et al.* Increased myocardial NAD(P)H oxidase-derived superoxide causes the exacerbation of postinfarct heart failure in type 2 diabetes. *Am J Physiol Heart Circ Physiol* 2009;**297**:H409–H416.
28. Nozaki N, Shishido T, Takeishi Y, Kubota I. Modulation of doxorubicin-induced cardiac dysfunction in toll-like receptor-2-knockout mice. *Circulation* 2004;**110**:2869–2874.
29. Dimri GP, Lee X, Basile G, Acosta M, Scott G, Roskelley C *et al.* A biomarker that identifies senescent human cells in culture and in aging skin *in vivo*. *Proc Natl Acad Sci USA* 1995;**92**:9363–9367.
30. Camelliti P, Borg TK, Kohl P. Structural and functional characterisation of cardiac fibroblasts. *Cardiovasc Res* 2005;**65**:40–51.
31. Yue TL, Wang C, Romanic AM, Kidy K, Keller P, DeWolf WE Jr *et al.* Staurosporine-induced apoptosis in cardiomyocytes: a potential role of caspase-3. *J Mol Cell Cardiol* 1998;**30**:495–507.
32. Aoki H, Kang PM, Hampe J, Yoshimura K, Noma T, Matsuzaki M *et al.* Direct activation of mitochondrial apoptosis machinery by c-Jun N-terminal kinase in adult cardiac myocytes. *J Biol Chem* 2002;**277**:10244–10250.
33. Weber KT, Brilla CG. Pathological hypertrophy and cardiac interstitium. Fibrosis and renin-angiotensin-aldosterone system. *Circulation* 1991;**83**:1849–1865.
34. Izumiya Y, Kim S, Izumi Y, Yoshida K, Yoshiyama M, Matsuzawa A *et al.* Apoptosis signal-regulating kinase 1 plays a pivotal role in angiotensin II-induced cardiac hypertrophy and remodeling. *Circ Res* 2003;**93**:874–883.
35. Mollnau H, Wendt M, Szocs K, Lassegue B, Schulz E, Oelze M *et al.* Effects of angiotensin II infusion on the expression and function of NAD(P)H oxidase and components of nitric oxide/cGMP signaling. *Circ Res* 2002;**90**:E58–E65.
36. Giordano FJ. Oxygen, oxidative stress, hypoxia, and heart failure. *J Clin Invest* 2005;**115**:500–508.
37. Olivetti G, Abbi R, Quaini F, Kajstura J, Cheng W, Nitahara JA *et al.* Apoptosis in the failing human heart. *N Engl J Med* 1997;**336**:1131–1141.

38. Ravassa S, Fortuno MA, Gonzalez A, Lopez B, Zalba G, Fortuno A *et al.* Mechanisms of increased susceptibility to angiotensin II-induced apoptosis in ventricular cardiomyocytes of spontaneously hypertensive rats. *Hypertension* 2000;**36**:1065–1071.
39. Park M, Sher YT, Gaussin V, Heyndrickx GR, Bartunek J, Resuello RR *et al.* Apoptosis predominates in nonmyocytes in heart failure. *Am J Physiol Heart Circ Physiol* 2009;**297**: H785–H791.
40. Yu R, Schellhorn HE. Recent applications of engineered animal antioxidant deficiency models in human nutrition and chronic disease. *J Nutr* 2013;**143**:1–11.
41. Jung KJ, Ishigami A, Maruyama N, Takahashi R, Goto S, Yu BP *et al.* Modulation of gene expression of SMP-30 by LPS and calorie restriction during aging process. *Exp Gerontol* 2004;**39**:1169–1177.
42. Inuzuka Y, Okuda J, Kawashima T, Kato T, Niizuma S, Tamaki Y *et al.* Suppression of phosphoinositide 3-kinase prevents cardiac aging in mice. *Circulation* 2009;**120**:1695–1703.
43. Maejima Y, Adachi S, Ito H, Hirao K, Isobe M. Induction of premature senescence in cardiomyocytes by doxorubicin as a novel mechanism of myocardial damage. *Aging Cell* 2008;**7**:125–136.

Cardiovascular Research (2013) **99**, 382–394
doi:10.1093/cvr/cvt106

Nuclear accumulation of androgen receptor in gender difference of dilated cardiomyopathy due to lamin A/C mutations

Takuro Arimura[1], Kenji Onoue[2,3,4], Yumiko Takahashi-Tanaka[1], Taisuke Ishikawa[1], Masayoshi Kuwahara[5], Mitsutoshi Setou[4,6,7], Shuji Shigenobu[8], Katsushi Yamaguchi[8], Anne T. Bertrand[9,10], Noboru Machida[11], Kazumi Takayama[11], Masayuki Fukusato[11], Ryo Tanaka[12], Satoshi Somekawa[2,3], Tomoya Nakano[2,3], Yoshihisa Yamane[12], Keiji Kuba[13], Yumiko Imai[13], Yoshihiko Saito[2,3], Gisèle Bonne[9,10,14], and Akinori Kimura[1]*

[1]Department of Molecular Pathogenesis, Medical Research Institute, Tokyo Medical and Dental University, 1-5-45 Bunkyo-Ku, Tokyo 113-8510, Japan; [2]First Department of Internal Medicine, Nara Medical University, Kashihara, Japan; [3]Department of Regulatory Medicine for Blood Pressure, Nara Medical University, Kashihara, Japan; [4]Department of Cell Biology and Anatomy, Hamamatsu University School of Medicine, Hamamatsu, Japan; [5]Department of Comparative Pathophysiology, Graduate School of Agriculture and Life Sciences, The University of Tokyo, Tokyo, Japan; [6]Systems Molecular Anatomy Laboratory, Medical Photonics Research Center, Hamamatsu University, School of Medicine, Hamamatsu, Japan; [7]National Institute for Physiological Sciences, Okazaki, Japan; [8]National Institute for Basic Biology, Okazaki, Japan; [9]INSERM, U974, Paris, France; [10]Université Pierre et Marie Curie-Paris 6, UM 76, CNRS, UMR 7215, Institut de Myologie, Paris, France; [11]Department of Veterinary Clinical Oncology, Faculty of Agriculture, Tokyo University of Agriculture and Technology, Tokyo, Japan; [12]Department of Veterinary Surgery, Faculty of Agriculture, Tokyo University of Agriculture and Technology, Tokyo, Japan; [13]Department of Biological Informatics and Experimental Therapeutics, Akita University Graduate School of Medicine, Japan; and [14]AP-HP, Groupe Hospitalier Pitié-Salpêtrière, U.F. Cardiogénétique et Myogénétique, Service de Biochimie Métabolique, Paris, France

Received 30 August 2012; revised 19 April 2013; accepted 24 April 2013; online publish-ahead-of-print 30 April 2013

Time for primary review: 27 days

Aims Dilated cardiomyopathy (DCM) is characterized by ventricular dilation associated with systolic dysfunction, which could be caused by mutations in lamina/C gene (*LMNA*). *LMNA*-linked DCM is severe in males in both human patients and a knock-in mouse model carrying a homozygous p.H222P mutation ($Lmna^{H222P/H222P}$). The aim of this study was to investigate the molecular mechanisms underlying the gender difference of *LMNA*-linked DCM.

Methods and results A whole-exome analysis of a multiplex family with DCM exhibiting the gender difference revealed a DCM-linked *LMNA* mutation, p.R225X. Immunohistochemical analyses of neonatal rat cardiomyocytes expressing mutant *LMNA* constructs and heart samples from the *LMNA*-linked DCM patients and $Lmna^{H222P/H222P}$ mice demonstrated a nuclear accumulation of androgen receptor (AR) and its co-activators, serum response factor, and four-and-a-half LIM protein-2. Role of sex hormones in the gender difference was investigated *in vivo* using the $Lmna^{H222P/H222P}$ mice, where male and female mice were castrated and ovariectomized, respectively, or treated with testosterone or an antagonist of AR. Examination of the mice by echocardiography, followed by the analyses of histological changes and gene/protein expression profiles in the hearts, confirmed the involvement of testicular hormone in the disease progression and enhanced cardiac remodelling in the $Lmna^{H222P/H222P}$ mice.

Conclusion These observations indicated that nuclear accumulation of AR was associated with the gender difference in *LMNA*-linked DCM.

Keywords Dilated cardiomyopathy • Gender difference • Androgen receptor • Testosterone • Lamin A/C

1. Introduction

Dilated cardiomyopathy (DCM), a primary cardiac muscle disorder characterized by ventricular chamber dilation and systolic dysfunction,[1] is the major cause of chronic heart failure (CHF) and the most common indication for cardiac transplantation.[2] Underlying aetiologies include genetic, viral, toxic agents like alcohol, mitochondrial, and metabolic disorders.[2] It is known that familial occurrence is seen in ~30–40% of

* Corresponding author. Tel: +81 3 5803 4905; fax: +81 3 5803 4907, Email: akitis@mri.tmd.ac.jp

Published on behalf of the European Society of Cardiology. All rights reserved. © The Author 2013. For permissions please email: journals.permissions@oup.com.

Downloaded from http://cardiovascres.oxfordjournals.org/ at Tokyo Medican and Dental University on March 5, 2014

DCM patients.[3] To date, mutations in more than 30 genes encoding components of sarcomere, sarcolemma, cytoskeletons, or nuclear envelope have been discovered in patients with DCM,[4] and 8% of familial and sporadic DCM may be caused by mutations in *LMNA* encoding lamin A/C.[5]

DCM occurs more frequently in men than in women (male to female ratio: 2.5),[6] and a recent study revealed significant gender differences in cardiac phenotypes such as a higher mortality and severer cardiac dysfunction in male DCM patients carrying *LMNA* mutation.[7] It has been suggested that gonadal hormones, such as testosterone and oestrogens, may explain the gender difference in cardiac phenotypes. Results from *in vitro* and *in vivo* studies suggest that oestrogen may play a pivotal role,[8,9] in part due to protective actions of female hormones, which was evidenced by increased cardiovascular risk in women after menopause and by cardiovascular benefits of oestrogen replacement therapy.[9] However, mechanisms for the gender difference in DCM remain unknown.

We have established a 'knock-in' mouse carrying a p.H222P mutation of *Lmna*.[10] Homozygous knock-in mice (*Lmna*$^{H222P/H222P}$) developed DCM phenotypes, including progressive left ventricular (LV) dilation and contractile dysfunction from 2 and 4 months of age in males and females, respectively.[10] *Lmna*$^{H222P/H222P}$ male mice displayed more prominent abnormalities in cardiac function than females, and they died of CHF between 4 and 10 months of age, while female mice died at 6 and 13 months of age,[10] indicating that the *Lmna*$^{H222P/H222P}$ mice are a good model for studying the gender difference in the *LMNA*-linked DCM. On the other hand, no gender difference was observed in another knock-in mouse model with a *LMNA* mutation, p.delK32,[11] suggesting that not all of *LMNA* mutations were associated with the gender difference.

In this study, we first identified a *LMNA* mutation, p.R225X, in a DCM family in which apparent gender difference in clinical course of DCM was observed. Transfection experiments of neonatal rat cardiomyocytes (NRCs) with the normal or mutant *LMNA* construct revealed that the p.R225X and p.H222P mutations induced nuclear accumulation of endogenous androgen receptors (AR), while such phenomena were not found with normal or p.delK32 mutation. The nuclear accumulation of AR was accompanied by testosterone-induced nuclear translocation of four-and-a-half LIM protein-2 (FHL2) and serum response factor (SRF), which were involved in the cardiac remodelling process. *In vivo* studies revealed the adverse effect of testosterone in the cardiac function and pathological changes in the heart of *Lmna*$^{H222P/H222P}$ mice. We report here the involvement of AR and testosterone as a molecular basis for the gender difference in the progression of DCM caused by specific *LMNA* mutations.

2. Methods

Experimental details including methods of anaesthesia are described in Supplementary Information.

2.1 Mutational analysis

All human subjects and tissues were collected in accordance with the principles outlined in the Declaration of Helsinki. Whole-exome and sequencing analyses were performed with genomic DNA samples obtained from the subjects after given informed consent. The protocol for research was approved by the Ethics Reviewing Committees of Medical Research Institute, Tokyo Medical and Dental University, and Nara Medical University.

2.2 Heart tissues

Paraffin-embedded LV myocardial tissues obtained at autopsy from three male patients with DCM carrying the p.R225X mutation, from two male patients with DCM carrying no *LMNA* mutation, and from two control subjects without DCM were analysed. Informed consent was given from relatives of each subject. Heart samples from the *Lmna*$^{H222P/H222P}$ [10] ($n = 4$), guanylyl cyclase A knock out (GC-A KO)[12] ($n = 3$), and transverse aortic constriction (TAC)[13] ($n = 2$) mice were prepared, as described previously.[10]

2.3 Immunofluorescence microscopy

All tissue sections and cells were prepared for immunofluorescence microscopy and analysed as described previously.[14,15]

2.4 Animals

Establishment of *Lmna*$^{H222P/H222P}$ mouse line was reported previously.[10] Mice were fed with a chow diet and housed in a barrier facility. All care and experimental procedures of animals were in accordance with the guidelines for the Care and Use of Laboratory Animals published by the National Institute of Health (NIH Publication, eighth edition, 2011) and subjected to prior approval by the local animal protection authority in Tokyo Medical and Dental University.

2.5 Castration and ovariectomy

Six-week-old male and female wild-type (WT, *Lmna*$^{+/+}$) and *Lmna*$^{H222P/H222P}$ mice before puberty underwent bilateral castration and ovariectomy, respectively, under anaesthesia.

2.6 Treatment with testosterone or flutamide

Castrated male mice ($n = 16$ and 20 of WT and *Lmna*$^{H222P/H222P}$ mice, respectively) and non-operated female mice ($n = 16$ and 21 of WT and *Lmna*$^{H222P/H222P}$ mice, respectively) were subcutaneously implanted with a 25 mm long silascon tube (inner diameter, 2.0 mm; outer diameter, 3.0 mm; Kaneka medix) containing crystalline testosterone under anaesthesia.[16] Non-operated male mice ($n = 16$ and 20 of WT and *Lmna*$^{H222P/H222P}$ mice, respectively) were also implanted subcutaneously with the tube containing crystalline flutamide, an AR antagonist (Sigma-Aldrich). Empty tubes were implanted in sham-operated animals (males: $n = 16$ and 19 of WT and *Lmna*$^{H222P/H222P}$ mice; females: $n = 16$ and 21 of WT and *Lmna*$^{H222P/H222P}$ mice, respectively). Testosterone- or flutamide-containing tubes were incubated in the saline at 37° for 24 h before implantation to avoid a surge-like release after implantation. The implanted tubes were not removed throughout the experiments.

2.7 Echocardiography, electrocardiography (ECG), and blood pressure measurement

Transthoracic echocardiography, electrocardiography (ECG) analysis, and measurement of systolic blood pressure and heart rate were performed, as described previously.[17,18]

2.8 Histopathological examinations

Histopathological examination using haematoxylin–eosin or Masson's trichrome staining was done by the standard methods ($n = 4$, each group). Measurement of interstitial fibrosis area and quantitative analysis of collagen in the heart were performed ($n = 6$, each group), as described previously.[18]

2.9 Ribonucleic acid (RNA) isolation and quantitative expression analysis

Total RNA extraction, complementary deoxyribonucleic acid (cDNA) synthesis, and real-time reverse transcription (RT)–polymerase chain reaction (PCR) analysis were performed ($n = 6$ in each group) as described previously.[18] Relative steady-state levels of messenger RNA (mRNA)

Downloaded from http://cardiovascres.oxfordjournals.org/ at Tokyo Medican and Dental University on March 5, 2014

were calculated using a comparative Ct (ΔδCT) method.[19] Individual expression values were normalized against the level of *Gapdh* mRNA.

2.10 Protein extraction and immunoblotting

Total cellular protein was extracted ($n = 4$, each group) as described previously.[15] Nuclear protein fraction was prepared ($n = 8$, each group) using NE-PER Nuclear and Cytoplasmic Extraction Regents (Pierce). Western blotting analysis was performed using primary antibodies against β-myosin heavy chain (βMHC), atrial natriuretic peptide (ANP), AR, SRF, FHL2, emerin, and glyceraldehyde 3-phosphate dehydrogenase (GAPDH) (Santa Cruz). The signal obtained for GAPDH was used as an internal control to normalize the amounts of protein on the immunoblots.

2.11 Measurement of serum testosterone level

Blood samples were obtained by heart puncture at time of necropsy and serum testosterone level was measured by radioimmunoassay using a DPC total testosterone kit (Mitsubishi chemical Medicine).

2.12 Statistical analysis

Phenotypic data were acquired by observers who were blinded to the genotype of mice. Numerical data were expressed as means ± SEM. Statistical differences were analysed using two-way analysis of variance (ANOVA) and then evaluated using a Tukey adjustment for the *post hoc* test. Survival curves were drawn for each group with the Kaplan–Meier method and the differences were compared by a log-rank test. A P-value <0.05 was considered to be statistically significant.

3. Results

3.1 Mutational analysis

We found a DCM family in which affected males had severer symptoms and phenotypes than females at the time of onset (*Figure 1* and see Supplementary material online, *Table S1*); all affected males had abnormalities both in cardiac conduction system and cardiac function at around the age of 30s to early 40s, whereas affected females had abnormalities in the cardiac conduction system at around the age of 40s and developed mild cardiac dysfunction later identified several sequence variations (see Supplementary material online, *Table S2*) including a *LMNA* mutation (c.673C>T, p.R225X) in the tested members, and a subsequent direct sequencing analysis revealed that all affected individuals and no unaffected members carried the p.R225X mutation, demonstrating a linkage of *LMNA* mutation to DCM with a LOD score of 3.01. This finding was consistent with that the *LMNA* mutations were associated with cardiac conduction disorder and gender difference in humans[7] and in *Lmna*$^{H222P/H222P}$.[10]

3.2 Accumulation of AR in nuclei of cardiomyocytes expressing LMNA with specific mutations

Because sexual hormones mediate their functions via specific receptor, we investigated whether the cellular localization of AR and estrogenic receptor (ER) α and β would be affected by specific *LMNA* mutations. We analysed NRCs transfected with Flag-tagged WT or mutant *LMNA* constructs carrying p.R225X, p.H222P, or p.delK32. Endogenous AR was found in both cytoplasm and nucleus in the cells expressing normal *LMNA* or *LMNA* with p.delK32, whereas increased nuclear accumulation of AR in the absence of androgen was observed in the most (~90%) of cells expressing *LMNA* with p.H222P or p.R225X (*Figure 2A*). In contrast, no apparent differences in the localization of ERα and ERβ were observed among the transfected NRCs (see Supplementary material online, *Figure S1*). On the other hand, nuclear accumulation of AR was not evident in HeLa cells transfected with the Flag-tagged WT or mutant LMNA constructs (see Supplementary material online, *Figure S2*). These observations implied that the cardiomyocyte-specific nuclear accumulation of AR was associated with specific *LMNA* mutations exhibiting the gender difference.

3.3 Nuclear accumulation of AR in the heart muscle

Because the findings in the transfection experiments might be due to the overexpression of *LMNA* with mutations, we next investigated whether the nuclear accumulation of AR could be found in the heart muscle carrying the *LMNA* mutations. AR was found mainly in the cytoplasm in heart samples from a control and a DCM patient without any *LMNA* mutations,

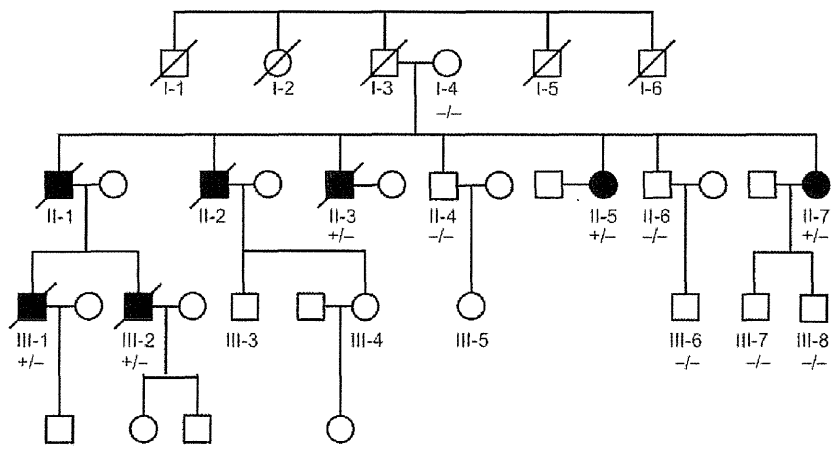

Figure 1 Pedigree tree of a DCM family Squares represent males; circles represent females. The presence (+/−) or absence (−/−) of the c.673C>T, p.R225X mutation in *LMNA* is indicated for the analysed subjects. Filled symbols indicate those with clinical symptoms and slashed indicate the deceased subjects.

Downloaded from http://cardiovascres.oxfordjournals.org/ at Tokyo Medican and Dental University on March 5, 2014

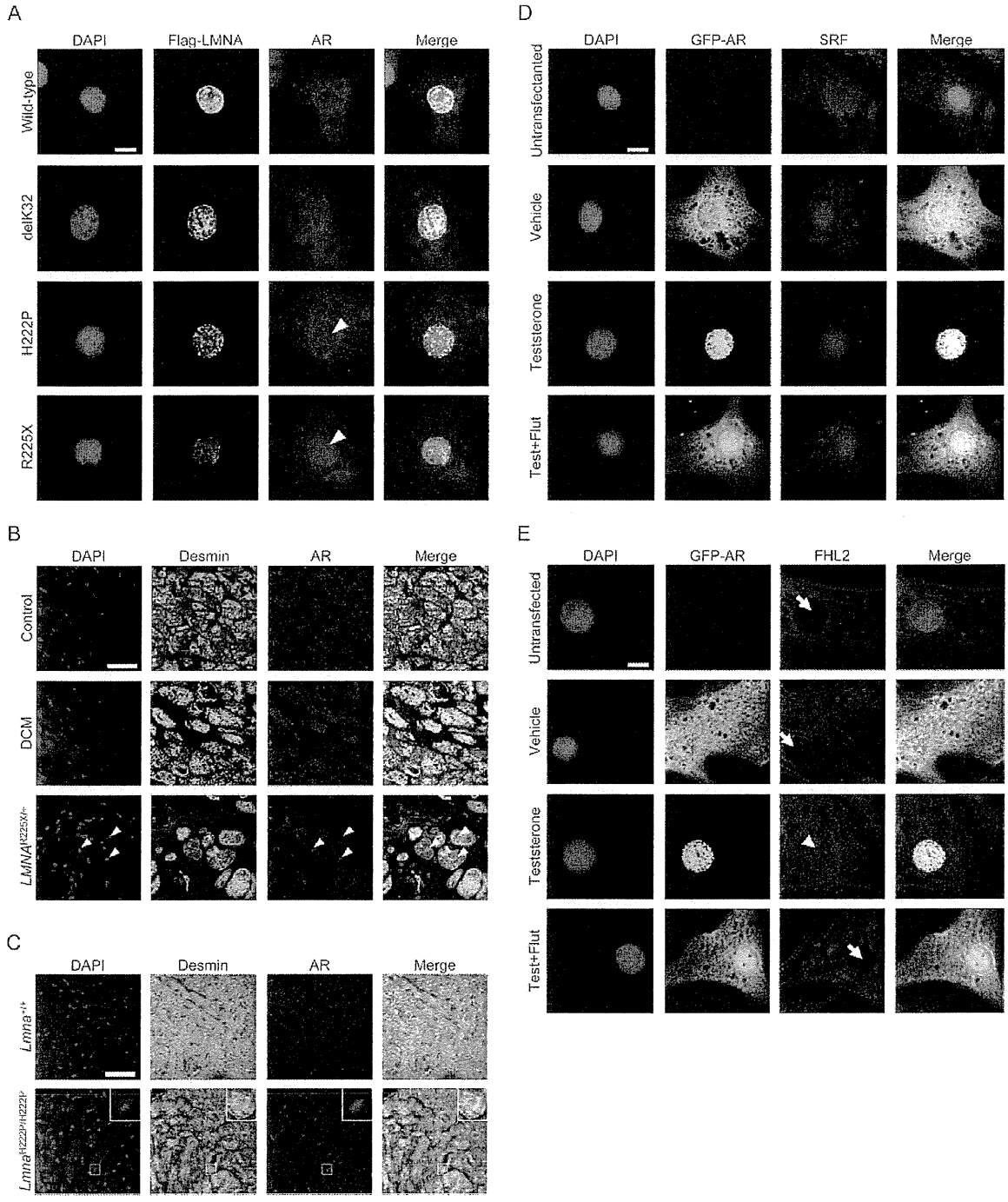

Figure 2 Localization of AR in cardiomyocytes. (*A*) NRCs transfected with Flag-tagged LMNA-WT, -p.delK32, -p.H222P, or -p.R225X construct were stained with DAPI, anti-Flag ,or anti-AR antibody. Merged images are also shown. Arrows indicate the accumulation of AR in nuclei; scale bars=10 μm. (*B*) Immunohistochemical analysis of AR in the hearts from a control subject, a DCM patient without *LMNA* mutation, and a DCM patient with p.R225X mutation. Immunostaining with anti-AR and -desmin antibodies shows localization of AR in the desmin-positive cardiomyocytes. Arrows indicate the representative nuclear accumulation of AR; scale bars=40 μm. Similar nuclear accumulation was found in two other DCM patients with the p.R225X. (*C*) Immunohistochemical analysis of AR in the hearts from *Lmna*$^{+/+}$ and *Lmna*$^{H222P/H222P}$ male mice at 6 months of age. Representative nuclear accumulation of AR was indicated as a high-magnification image. Nuclei in each tissue section were stained with DAPI; scale bars=40 μm. (*D* and *E*) Untransfected NRCs or NRCs transfected with GFP-tagged AR construct were treated with vehicle (0.01% ethanol), testosterone (1 μM), or testosterone (1 μM) plus flutamide (10 μM) 48 h after the transfection, fixed, and stained with DAPI and anti-SRF (*D*) or anti-FHL2 (*E*) antibody. Merged images are also shown. Arrows and arrowheads indicate the absence and presence, respectively, of GFP-AR in nuclei; scale bars=10 μm. Test +Flut; testosterone plus flutamide treated.

Downloaded from http://cardiovascres.oxfordjournals.org/ at Tokyo Medican and Dental University on March 5, 2014

whereas the nuclear localization of AR was obviously increased in the heart samples from patients with p.R225X mutation (*Figure 3B*) and *Lmna*$^{H222P/H222P}$ mice (*Figure 3C* and see Supplementary material online, *Figure S3a*). We also investigated whether or not the nuclear accumulation of AR was observed in the hearts from GC-A KO mice[12] and TAC-operated mice,[13] because they were mouse models for cardiac hypertrophy, of which male mice showed more prominent cardiac phenotypes. However, no apparent change in the localization of AR was observed in both mouse models (see Supplementary material online, *Figure S4*), indicating that the nuclear AR accumulation in the cardiomyocytes was associated with specific *LMNA* mutations. In addition, accumulation of AR co-factors, SRF and FHL2, which are known to be involved in the cardiac remodelling,[20,21] was observed in the nuclei of hearts from the male patients with p.R225X (see Supplementary material online, *Figure S5*). Furthermore, the nuclear accumulation of SRF and FHL2 was observed in the hearts from male *Lmna*$^{H222P/H222P}$, but not from female mice (see Supplementary material online, *Figures S3* and *S6*). It was therefore confirmed *in vivo* that the nuclear accumulation of AR was accompanied by the nuclear translocation of SRF and FHL2 in male hearts with specific *LMNA* mutations.

3.4 Nuclear translocation of FHL2 and SRF in NRCs

The role of AR in nuclear accumulation of FHL2 and SRF was investigated in NRCs transfected with GFP-tagged AR in the presence or absence of testosterone or an AR antagonist, flutamide. GFP-AR and SRF were observed in both cytoplasm and nucleus (*Figure 2D*), while FHL2 was found specifically in the cytoplasm in the most (~90%) of transfected NRCs (*Figure 2E*). Upon treatment with testosterone, both GFP-AR and SRF translocated to nuclei, whereas FHL2 displayed partial nuclear localization in ~80% of the transfected NRCs. On the other hand, the testosterone-induced nuclear accumulation of AR, SRF, and FHL2 was suppressed by flutamide. In addition, silencing of *FHL2* by siRNA in NRCs expressing GFP-AR revealed that the preferential nuclear localization of SRF in testosterone-treated cells was mediated by FHL2 (*Figure 3*).

3.5 Survival prognosis of Lmna$^{H222P/H222P}$ mice with removal of gonadal organs

The role of sex hormones in the mortality and severity of *LMNA*-linked DCM was investigated *in vivo*, where male and female WT (*Lmna*$^{+/+}$) and *Lmna*$^{H222P/H222P}$ mice were castrated and ovariectomized, respectively (see Supplementary material online, *Figure S7*). We found that the castration significantly improved survival prognosis of male *Lmna*$^{H222P/H222P}$ mice, as evidenced by the prolonged 50% survival time (8.09 $\pm$ 0.27 vs. 10.25 $\pm$ 0.38 months, $P < 0.001$) and reduced overall mortality ($P < 0.001$, log-rank test) (*Figure 4A*). Improvement in mortality observed with ovariectomized *Lmna*$^{H222P/H222P}$ female mice was not statistically significant ($P = 0.10$), but the 50% survival time was significantly prolonged by the ovariectomy (10.10 $\pm$ 0.28 vs. 11.07 $\pm$ 0.32 months, $P < 0.05$) (*Figure 4A*). These data demonstrated the beneficial effect of removing gonadal organs on the survival prognosis of *Lmna*$^{H222P/H222P}$ mice especially in male mice and to only a little extent in female mice.

3.6 Evaluation of cardiac function in Lmna$^{H222P/H222P}$ mice with removal of gonadal organs

Cardiac function was evaluated by using transthoracic echocardiography for sham-operated and operated mice at 3–4, 6–7, and 9–10 months of age (see Supplementary material online, *Figure S7*). The sham-operated *Lmna*$^{H222P/H222P}$ mice, in both male and female, showed progressive LV dilation and contractile dysfunction, as indicated by the decreased LV fractional shortening (LVFS) and LV ejection fraction (LVEF). The castration preserved LVFS and LVEF in males, whereas the ovariectomy showed no significant impact in females (*Table 1*, see Supplementary material online, *Figure S8*). When we measured blood pressure of sham-operated and castrated *Lmna*$^{H222P/H222P}$ male mice at 4 months of age by the indirect tail-cuff method, the systolic blood pressure was not significantly changed by the castration; sham-operated 121.0 $\pm$ 3.7 vs. castrated 126.2 $\pm$ 4.0 mmHg ($n = 6$ in each group). These data demonstrated that the castration improved LV contractile dysfunction without affecting systolic blood pressure in the *Lmna*$^{H222P/H222P}$ mice. As for data of ECG, QRS complex duration and PR interval were prolonged, albeit not significant, in the *Lmna*$^{H222P/H222P}$ mice, in both male and female, as reported previously,[10] but there were no changes by the castration or ovariectomy (see Supplementary material online, *Table S3*).

To directly demonstrate the role of androgen in disease progression, we treated mice with testosterone or flutamide. By the testosterone treatment, cardiac dysfunction was accelerated in the castrated male *Lmna*$^{H222P/H222P}$ mice. In contrast, progression of cardiac dysfunction was slowed in the flutamide-treated male *Lmna*$^{H222P/H222P}$ mice (*Table 2*).

3.7 Histopathological study of hearts from Lmna$^{H222P/H222P}$ mice

Histopathological analyses of the hearts demonstrated the ventricular dilation with enlarged atrial cavity often accompanied by atrial thrombus in the sham-*Lmna*$^{H222P/H222P}$ mice. These abnormalities were also observed in the testosterone-treated female *Lmna*$^{H222P/H222P}$ mice as well as in the castrated and testosterone-treated male *Lmna*$^{H222P/H222P}$ mice (*Figure 4B*). Either castration or flutamide treatment prevented the development of CHF with congestive lung in the male *Lmna*$^{H222P/H222P}$ mice. Prominent interstitial fibrosis, degeneration, and necrosis of single and/or a small cluster of cardiomyocytes were found in the ventricles of sham-operated male *Lmna*$^{H222P/H222P}$, testosterone-treated castrated male *Lmna*$^{H222P/H222P}$, and testosterone-treated female *Lmna*$^{H222P/H222P}$ mice, but these abnormalities were suppressed in the castrated or flutamide-treated mice (*Figure 4B*). In addition, quantitative analyses of myocardial interstitial fibrosis demonstrated that the collagen deposits were significantly increased in the hearts from sham-operated male *Lmna*$^{H222P/H222P}$ mice, which was significantly suppressed by the castration or flutamide treatment (*Figure 4C* and *D*). These observations indicated that deprivation or blockage of testosterone-related signals inhibited the interstitial fibrosis in the *Lmna*$^{H222P/H222P}$ hearts.

Downloaded from http://cardiovascres.oxfordjournals.org/ at Tokyo Medican and Dental University on March 5, 2014

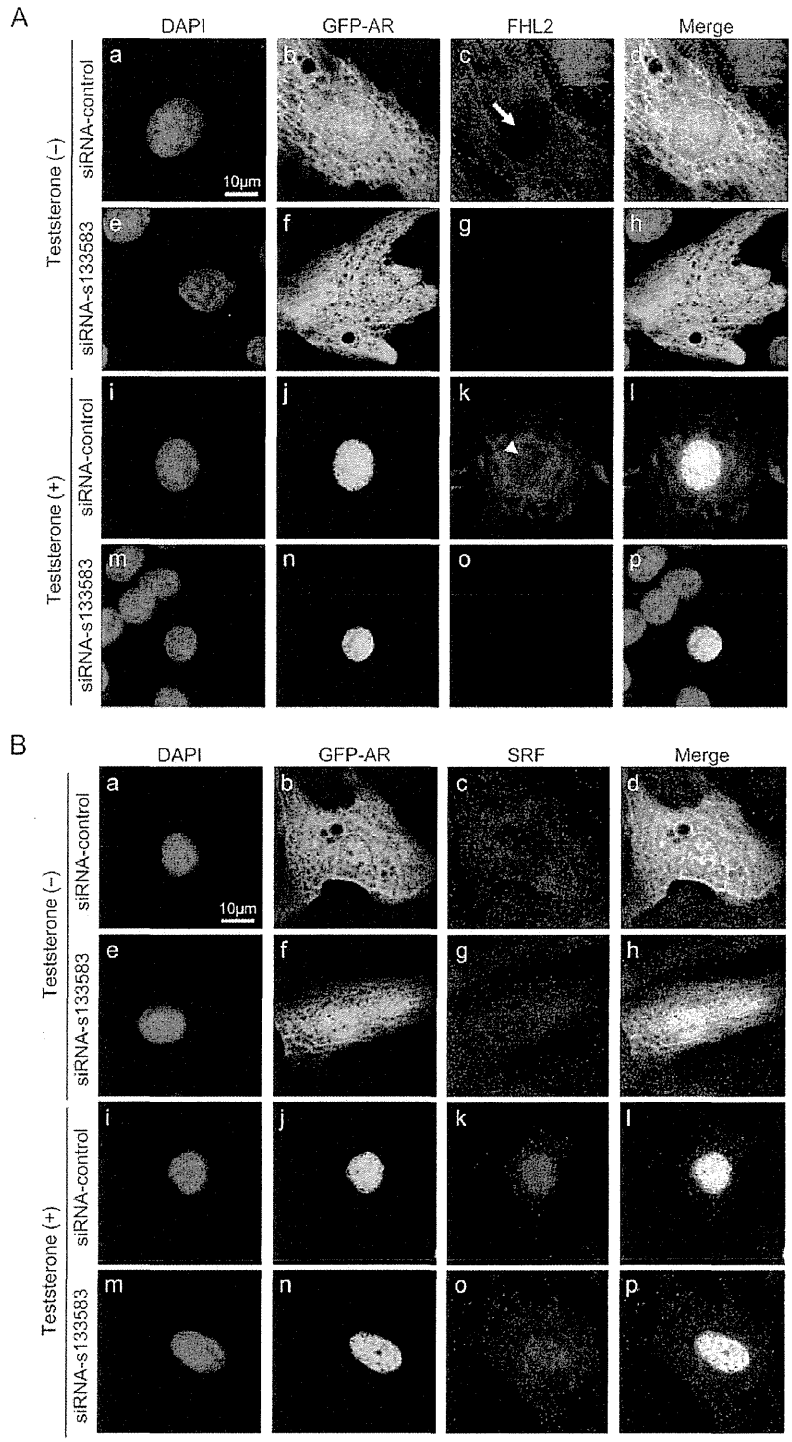

Figure 3 Effect of FHL2 silencing on localization of SRF in NRCs transiently expressed GFP-tagged AR and treated with testosterone. NRCs co-transfected with GFP-tagged AR construct and non-silencing (*a–d and i–l*), or pre-designed (e–*h* and *m–p*) siRNA were treated without (*a–d* and e–*h*) or with (*i–l* and *m–p*) testosterone (1 μM) 48 h after the transfection. The cells were fixed and stained with DAPI (*a*, e, *i*, and *m*) and anti-FHL2 (*c, g, k,* and *o* in *A*) or anti-SRF (*c, g, k,* and *o* in *B*) antibody. Merged images are shown in *d, h, l,* and *p*. Arrow and arrowhead indicate the absence and presence, respectively, of FHL2 in nuclei; scale bars=10 μm.

Downloaded from http://cardiovascres.oxfordjournals.org/ at Tokyo Medican and Dental University on March 5, 2014

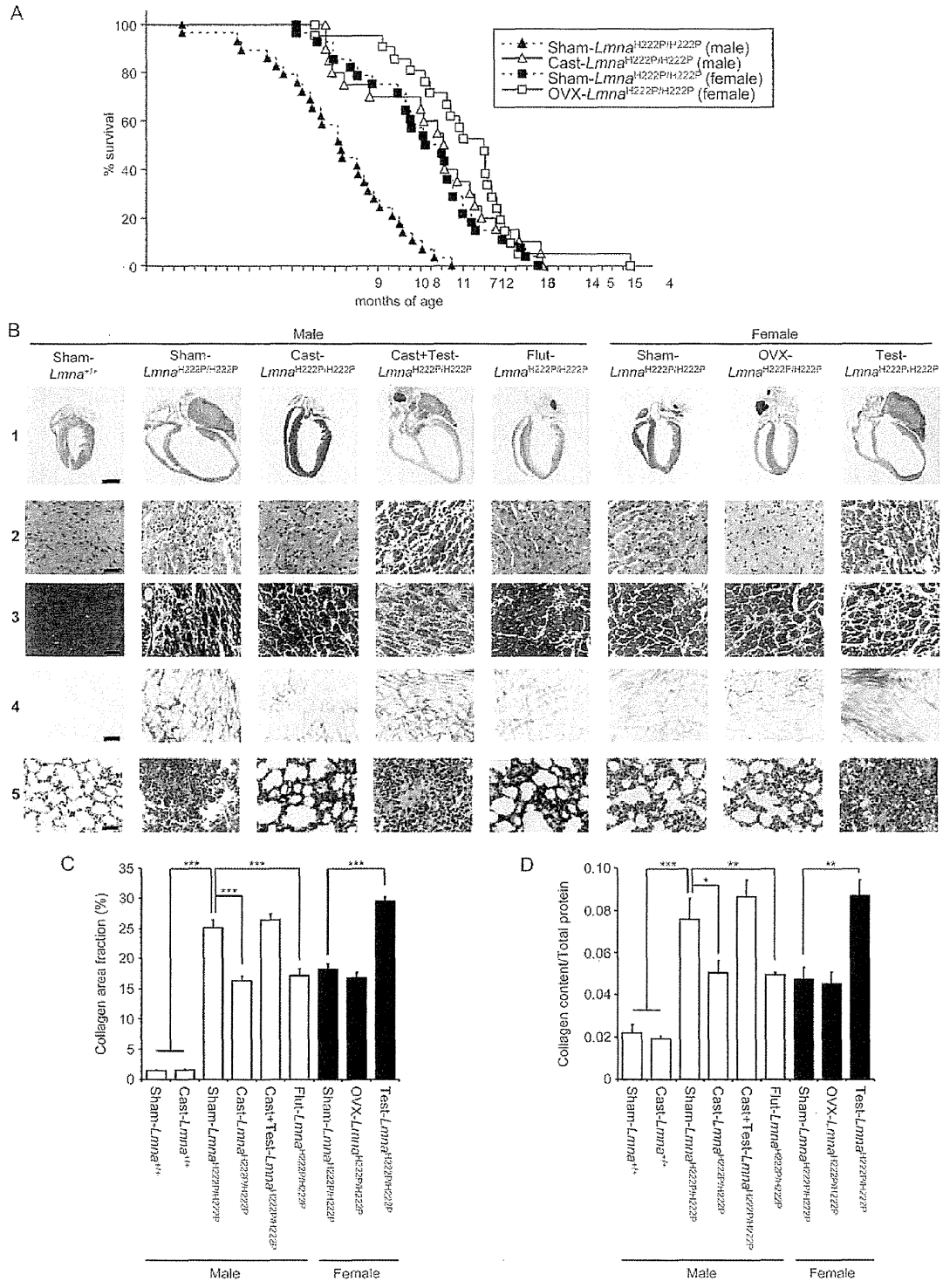

Figure 4 Disease expression of sham-operated and operated *Lmna*$^{H222P/H222P}$ mice. (*A*) Cumulative survival curves are indicated for sham-operated (Sham) male (closed triangles, $n = 29$) and female (closed squares, $n = 28$) mice, and castrated (Cast) male (open triangles, $n = 20$) and ovariectomized (OVX) female (open squares, $n = 21$) mice. (*B*) Pathological analyses of heart and lung; (1) longitudinal sections through the atria and ventricles of male and female mice at 6 months of age; scale bar=2 mm. Histopathological analysis of the LV with H&E staining (2), Masson's trichrome staining (3), or picrosirius red staining (4) and the lung with H&E staining (5); scale bars=50 μm except that in (4) =100 μm. (*C*) Quantitative measurement of myocardial collagen area fraction from five pictures per cross-section expressed as percentage of collagen staining to total area. Data are represented as means ± SEM for $n = 4$ to 6 per group. (*D*) Quantitative analysis of collagen content in the ventricles. Data are represented as means ± SEM for $n = 4$ to 6 per group. $^{*}P < 0.05$, $^{**}P < 0.01$, and $^{***}P < 0.001$. Sham: sham-operated, Cast: castrated, Cast+Test: castrated and testosterone-treated, Flut: flutamide-treated.

Downloaded from http://cardiovascres.oxfordjournals.org/ at Tokyo Medican and Dental University on March 5, 2014